Electronic Supplementary Information (ESI) for

Asymmetric dual species copper (II/I) electrolyte dye-sensitized solar cells with 35.6% efficiency under indoor light

Sruthi Meledath Meethal [a,c], Sourava Chandra Pradhan [a,c], Jayadev Velore [a,c], Sunil Varughese [b,c], Renjith S. Pillai [d], Frédéric Sauvage [e], Anders Hagfeldt [f] and Suraj Soman*[a,c]

[a] Centre for Sustainable Energy Technologies (C-SET), CSIR-National Institute for Interdisciplinary Science and Technology (CSIR-NIIST), Thiruvananthapuram 695019, India.
[b] Chemical Sciences and Technology Division, CSIR-National Institute for Interdisciplinary Science and Technology (CSIR-NIIST), Thiruvananthapuram 695019, India.
[c] Academy of Scientific and Innovative Research (AcSIR), Ghaziabad-201002, India.
[d] Analytical and Spectroscopy Division, Vikram Sarabhai Space Centre, Indian Space Research Organisation (ISRO), Thiruvananthapuram 695 022, India.
[e] Laboratoire de Réactivité et Chimie des Solides (LRCS), CNRS UMR 7314, Université de Picardie Jules Verne, 15 Rue Baudelocque, 80039 Amiens, France.
[f] Department of Chemistry–Ångström Laboratory, Uppsala University, Uppsala SE-75120, Sweden.

Email: suraj@niist.res.in

Table of contents

Experimental section

Materials

CuI (Sigma-Aldrich), $CuCl_2$ (Sigma-Aldrich), neocuproine hydrate (Sigma-Aldrich), lithium bis (trifluormethanesulfonyl)imide (LiTFSI) (TCI), 6,6'-dimethyl-2,2'-dipyridyl (dmby) (Sigma-Aldrich), ferrocene (Sigma-Aldrich), tetrabutylammonium hexafluorophosphate ($TBAPF_6$) (Sigma-Aldrich), 4-tert-Butylpyridine (tBP) (Sigma-Aldrich), titanium(IV) chloride ($TiCl_4$) (Sigma-Aldrich), isopropanol (IPA) (Merck), acetonitrile (Merck), ethanol (Merck), Fluorine doped tin oxide (FTO) (TEC 15 and TEC 8, GreatCell Solar (Australia)), titanium dioxide (TiO_2) (18NRT, and 18NR-AO, GreatCell Solar), surlyn (thickness-25µm, GreatCell Solar), UV epoxy resin (TB3035B) (ThreeBond), organic photosensitisers (Y123, D35 and XY1) (Dyenamo AB (Stockholm, Sweden)).

(I) Synthesis of copper complexes: $[Cu(I)(dmp)_2]^+$, $[Cu(I)(dmby)_2]^+$ and $[Cu(II)(dmby)_2]^{2+}$ were synthesized by following previous literature procedures. [1,2]

Synthesis of Cu(II) complexes:

(a) synthesis of $[Cu(II)(dmp)_2]^{2+}$

$[Cu(II)(dmp)_2]^{2+}$ was synthesised by mixing one equivalent of nitrosonium tetrafluoroborate ($NOBF_4$) (108.5 mg, 0.93 mmol) to an acetonitrile solution containing $[Cu(I)(dmp)_2](TFSI)$ (446 mg, 0.93 mmol) under nitrogen atmosphere and the solution was stirred well for 30 minutes at room temperature. An immediate colour change from orange to green was noticed upon adding $NOBF_4$. 5 eq. of lithium bis(trifluoromethane sulfonyl)imide (LiTFSI) (133.4 mg, 0.65 mmol) was then added and stirred for 2 hours. The solvent was removed by rotatory evaporation, and the crude sample was dissolved in a minimum amount of dichloromethane. The complex was collected by filtration after precipitation using diethyl ether. Bright violet powder of $[Cu(II)(dmp)_2]^{2+}$complex was obtained with 32% yield (305 mg).

(b) Synthesis of $[Cu(II)(dmp)_2Cl]^+$

To an oven-dried flask containing neocuproine hydrate (155 mg, 0.74 mmol), a 2:1 mixture of water and methanol was added and heated at 70 ^oC until the ligands were completely dissolved. The solution was then cooled to 50 ^oC, and $CuCl_2$ (50 mg, 0.37 mmol) was added and stirred for 10 minutes. Finally, LiTFSI (5 equivalents) in water (10 ml) was added and stirred at 50 ^oC for one hour. The solid green product was collected by vacuum filtration and washed with water, and dried to get $[Cu(II)(dmp)_2Cl]^+$. Yeild = 91% (270 mg). Single crystals of $[Cu(dmp)_2Cl]^+$ and tBP coordinated Cu(II) dmp complexes are obtained by slow diffusion of ether to a saturated solution of $[Cu(dmp)_2Cl]^+$ and $[Cu(dmp)_2Cl]^+$ with 15 equivalent of tBP in acetonitrile solutions respectively.

(c) Analogous $[Cu(II)(dmby)_2Cl]^+$ complex was synthesized by following similar method. Yeild - 86.3% (238.7 mg).

(II) Optical, electrochemical, XPS and NMR characterization of copper complexes

The absorption spectra of Cu complexes were recorded using PerkinElmer UV/VIS/NIR Spectrometer Lambda 950 instrument from 250 nm to 1200 nm using acetonitrile as solvent. The electrochemical characterisation was carried out using Bio-Logic VSP potentiostat using a three-electrode setup consisting of glassy carbon as the working electrode, Pt as the counter electrode and Ag/AgCl as the reference electrode. All electrochemical measurements were performed in acetonitrile solution containing 0.1 M $TBAPF_6$ as supporting electrolyte at a scan rate of 100 mV/s. Ferrocene/Ferrrocenium (Fc/Fc+) redox couple with an $E_{1/2}$ = 0.395 V *vs* NHE was used as an internal standard. The oxidation state of Cu species was determined by an XPS spectrometer (ESCALAB 250Xi Thermo Scientific Escalab, USA) using AlKα radiation as the excitation source. Bruker AMX 500 spectrophotometer was used to record the ^{1}H-NMR spectrum in CD_3CN.

(III) Computational modelling and single crystal measurements of copper complexes

The geometry of the complexes is initially optimised using PBEPBE functional by Quickstep module of the CP2K package.[3] All the periodic-DFT calculations are performed by Unrestricted Kohn-sham (UKS) with spin multiplicity.[4] A triple zeta (TZVP-MOLOPT) basis set was considered for the elements such as carbon, chlorine, nitrogen, and hydrogen, but an SDD basis set was followed for copper.[5] Additionally, the van der walls corrections were applied by the DFT-D3 method and optimised by considering in gas phase within a cubic simulation box.[6] Single crystal X-ray analysis (SCXRD) were performed using Bruker Kappa APEXII CCD Diffractometer using graphite monochromated Mo-Kα radiation (0.71073 Å). The structure was solved by direct methods using OLEX2 programme package.

(IV) Dye-sensitized solar cell fabrication

All devices were fabricated using our existing dye-sensitized solar cell/module semi-automated fabrication facility (Fig. S29, ESI). One batch consists of 12 devices and 3 consecutive batches were done for each condition to calculate the error. For the working electrode, the fluorine doped tin oxide (FTO) glass substrates (TEC 15, GreatCell Solar) were cleaned with soap solution, deionised water (DI), acetone and isopropanol successively using an ultrasonic bath and annealed at 500 ^{o}C for 15 minutes. Further, the organic contaminants were removed by UV-Ozone treatment for 15 minutes. A compact TiO_2 blocking layer was coated on electrodes by immersing them in 53 mM $TiCl_4$ solution at 70 ^{o}C for 30 minutes, rinsing with DI water and ethanol, and annealing at 500 ^{o}C. The mesoporous TiO_2 layer (18NRT, Greatcell Solar) was screen printed and annealed at 100 ^{o}C for 10 minutes; further scattering layer (18NR-AO TiO_2) was printed over the active layer followed by annealing at 500 ^{o}C for 30 minutes. The total thickness of TiO_2 was found to be 8 µm measured using a Dektak XT stylus profilometer. Finally, post blocking layer was deposited by $TiCl_4$ (40 mM) treatment as done for the pre-blocking layer. The counter electrodes were prepared by cleaning FTO glass plates (TEC 8, GreatCell Solar) having pre-drilled holes with soap solution, DI water and ethanol using an ultrasonic bath. The cleaned electrodes were annealed at 500 ^{o}C for 15 minutes, followed by UV-Ozone treatment for 15 minutes. A thin porous layer of poly(3,4-ethylene dioxythiophene) (PEDOT) was electrochemically deposited onto the conducting surface of FTO and was washed and dried. The dye solution was prepared by mixing 0.1 mM Y123 in a 1:1 acetonitrile: tert-butanol solvent. The co-sensitized dye solution of D35 and XY1 was prepared by mixing 0.1 mM of each dye in 1:1 acetonitrile and tert-butanol. Working electrodes were heated at 60 °C, immersed in the dye solution for 15 hours, and stored under dark conditions. The working and counter electrodes were then assembled using a 25 µm thick thermoplastic sealant material (Surlyn, Greatcell Solar). Copper electrolyte consisting of 0.2 M Cu(I), 0.04 M Cu(II), 0.1 M LiTFSI and 0.6 M tBP in acetonitrile solution was then injected into the device through the pre-drilled holes on the counter electrode and finally, sealed using a microscopic cover glass. For the direct contact devices, edges were sealed using UV-curable epoxy (3035B) obtained from ThreeBond.

(V) Dye-sensitized solar cell characterization

Current density-voltage (*J-V*) characteristics of fabricated devices were recorded using Oriel (Model PVIV-94043A) Class-AAA solar simulator connected with Keithley E 2400 source meter. The irradiation intensity was measured using a standard calibrated Si solar cell (Newport, USA). A black mask (0.1133 cm^2) was used during all the *J-V* measurements to avoid stray light. The devices' incident photon-to-current conversion efficiency (IPCE) was measured in DC mode using a 350 W Xenon lamp integrated Newport IPCE equipment with a monochromator and power meter (1918-R). The electrochemical impedance spectroscopy (EIS), open circuit voltage decay (OCVD) and the current transient measurements were performed using Metrohm Autolab (PGSTAT 302N). EIS of symmetrical dummy cells were carried out at 0 V with the perturbation of amplitude of 10 mV in the frequency range of 100 mHz to 100 kHz. Nyquist plots were fitted with equivalent circuit using Z-view software. Current transient measurements were performed at different light intensities ranging from 0.1 sun to 1 sun. Lifetime measurements for different days were obtained from transient photovoltage decay using the Dyenamo toolbox (DN-AE01). Charge extraction was measured using the Dyenamo toolbox setup. Photo-induced absorption spectroscopy (PIA) was measured using the Dyenamo PIA instrument (DN-AE02). Here 1W blue light-emitting LED (λ=470 nm) is used as a pump source, while a 20 W tungsten halogen lamp is used as a probe source. The transmitted light passes through the sample and monochromator and is detected by a UV-enhanced Si detector connected to a lock-in amplifier (SR830) via a current amplifier.

(VI) Indoor photovoltaic characterizations

Photovoltaic performance under indoor illumination was performed in a custom-designed indoor light measurement setup (Fig. S19, ESI). The reported photovoltaic data were obtained from the measurement of eight devices, and error values were computed using the standard deviation method. The indoor photovoltaic measuring set-up consists of various indoor light sources, Dyenamo potentiostat (DN-AE05), Ocean optics spectrometer (WW-83500-20), lux meter and a black box. Inside the black box, *J-V* measurements were carried out. We used four different lights for indoor PV measurements, which include daylight CFL (DL CFL), warm white CFL (WW CFL), daylight LED (DL LED) and warm white LED (WW LED). On the top of the black box, nine holders are placed at equidistance to mount desired indoor light source. The device under measurement is kept in the movable platform. A diffuser between the platform and light mount is placed to maintain the uniformity of light with better precision at lower illumination intensities. The platform can be moved precisely with a minimum of 1 mm per step, controlled with an HMI (Human-Machine Interface) attached to the black box. The desired intensity can be obtained by moving the platform. Illuminance in lux was measured using a lux meter, and the intensity in $\mu W/cm^2$ was measured using Ocean optics Jaz spectrometer (WW-83500-20) with an optical fiber and was further cross-verified using Dyenamo highly sensitive irradiance measuring unit (DN-AE06). The power spectra of these indoor light sources were measured using a spectrometer, and their integrated values are provided in Fig. S20, ESI and Table S1, ESI. *J-V* characteristics were measured using a Dyenamo IV measuring unit (DN-AE05) controlled by a computer through the IV software.

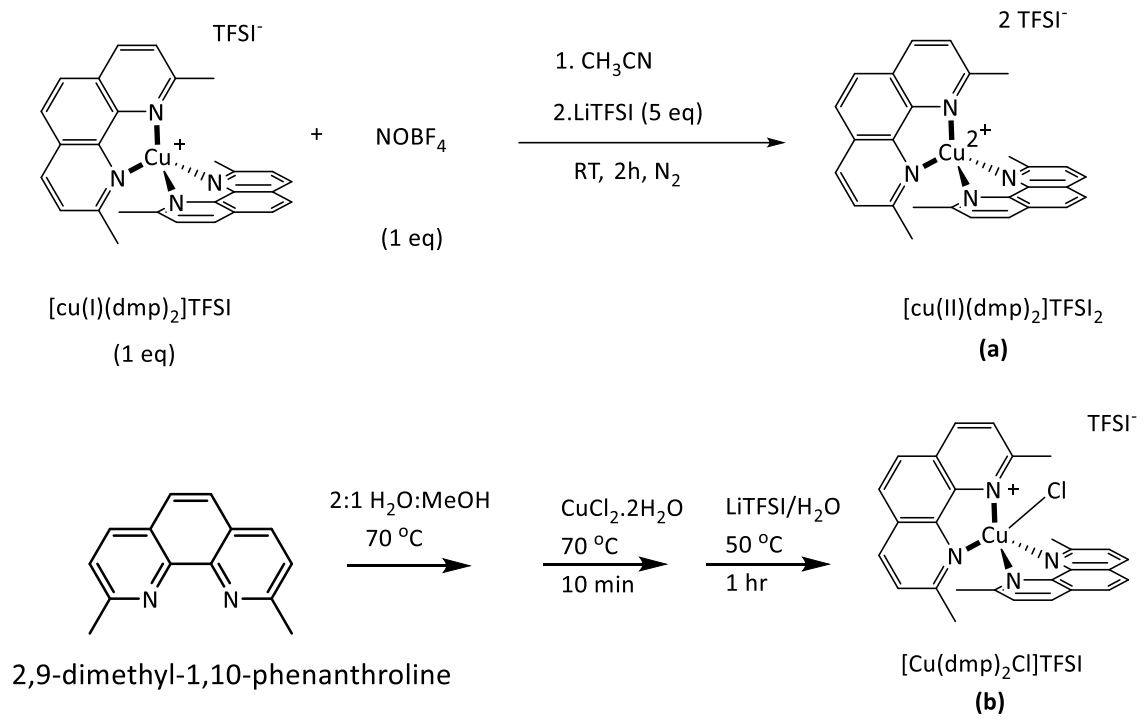

Fig. S1 Schematic representation of the synthesis of Cu(II) complexes.

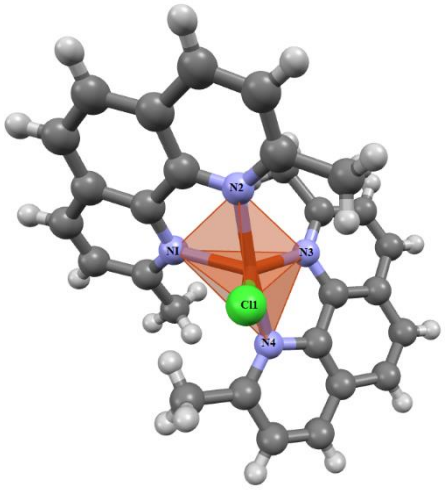

Fig. S2 Single crystal X-ray structure of five coordinated $[Cu(II)(dmp)_2Cl]^+$ complex.

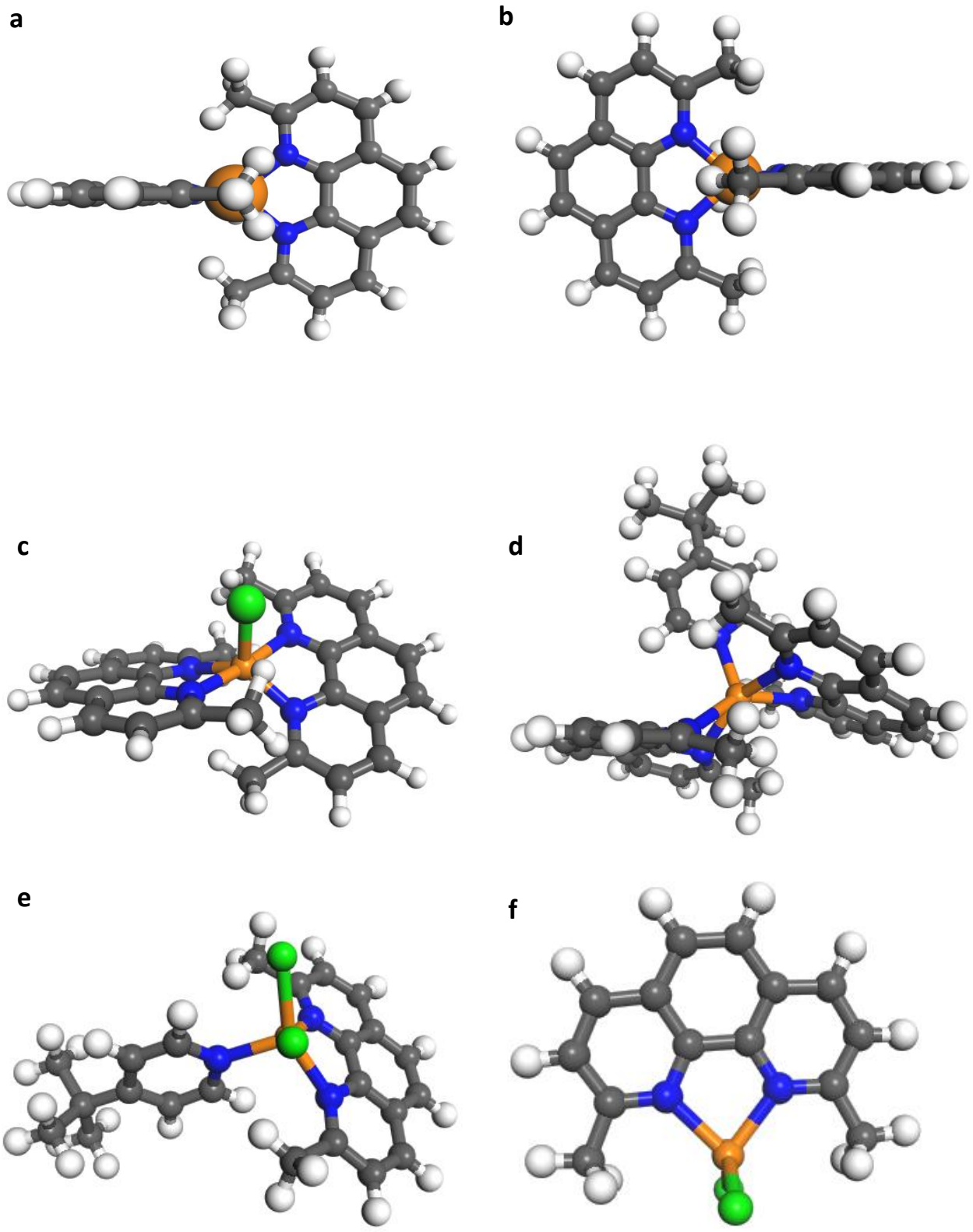

Fig. S3 DFT optimized structures of copper complexes (a) $[Cu(I)(dmp)_2]^+$, (b) $[Cu(II)(dmp)_2]^{2+}$,(c) $[Cu(II)(dmp)_2Cl]^+$,(d) $[Cu(II)(dmp)_2tBP]^{2+}$, (e) $[Cu(II)(dmp)(Cl)_2tBP]$, (f) $[Cu(I)(dmp)(Cl)_2]$.

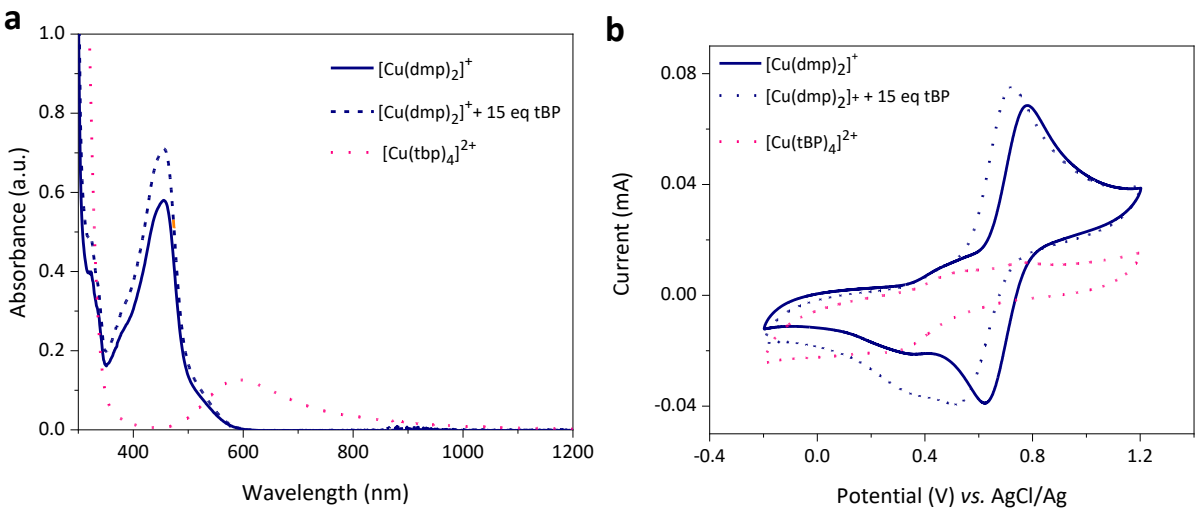

Fig. S4 (a) UV-Visible absorption spectra of $[Cu(dmp)_2]^+$, $[Cu(dmp)_2]^+$ in presence of 15 equivalent of tBP and $[Cu(tbp)_4]^{2+}$ in acetonitrile. (b) Cyclic voltammogram of 3 mM solution of $[Cu(dmp)_2]^+$, $[Cu(dmp)_2]^+$ in presence of 15 equivalent of tBP and $[Cu(TBP)_4]^{2+}$ in presence of 0.1M $TBAPF_6$/acetonitrile measured at 100 mV/s scan rate.

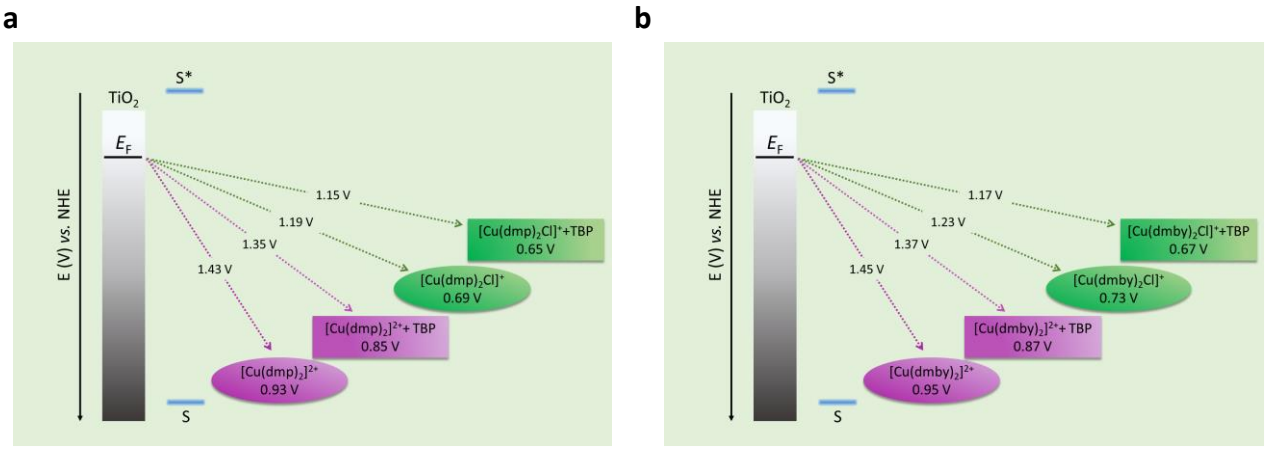

Fig. S5 Energy level diagram of phenanthroline and bipyridyl ligand coordinated Cu(II) complexes (a) $[Cu(dmp)_2]^{2+}/[Cu(dmp)_2Cl]^{+}$, (b) $[Cu(dmby)_2]^{2+}/[Cu(dmby)_2Cl]^{+}$ in the absence and presence of tBP with respect to the conduction band of TiO_2 and HOMO-LUMO level of sensitizer representing the difference in driving force for recombination between these electrolytes.

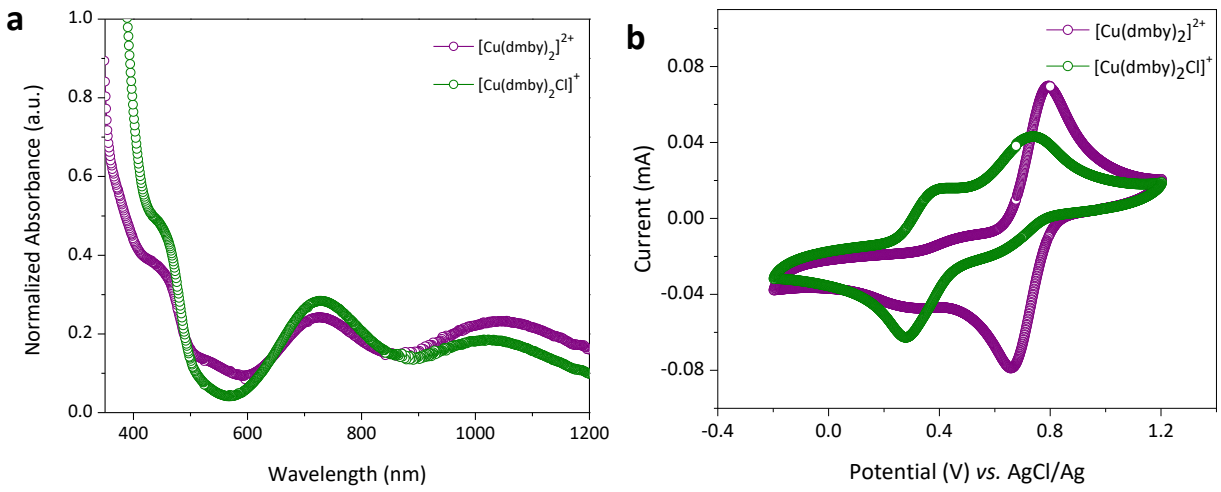

Fig. S6 (a) UV-Visible absorption spectra of $[Cu(dmby)_2]^{2+}$ and $[Cu(dmby)_2Cl]^{+}$ in acetonitrile solution. (b) Cyclic voltammogram of 3 mM $[Cu(dmby)_2]^{2+}$ and $[Cu(dmby)_2Cl]^{+}$ in presence of 0.1 M $TBAPF_6$/acetonitrile measured at 100 mV/s scan rate.

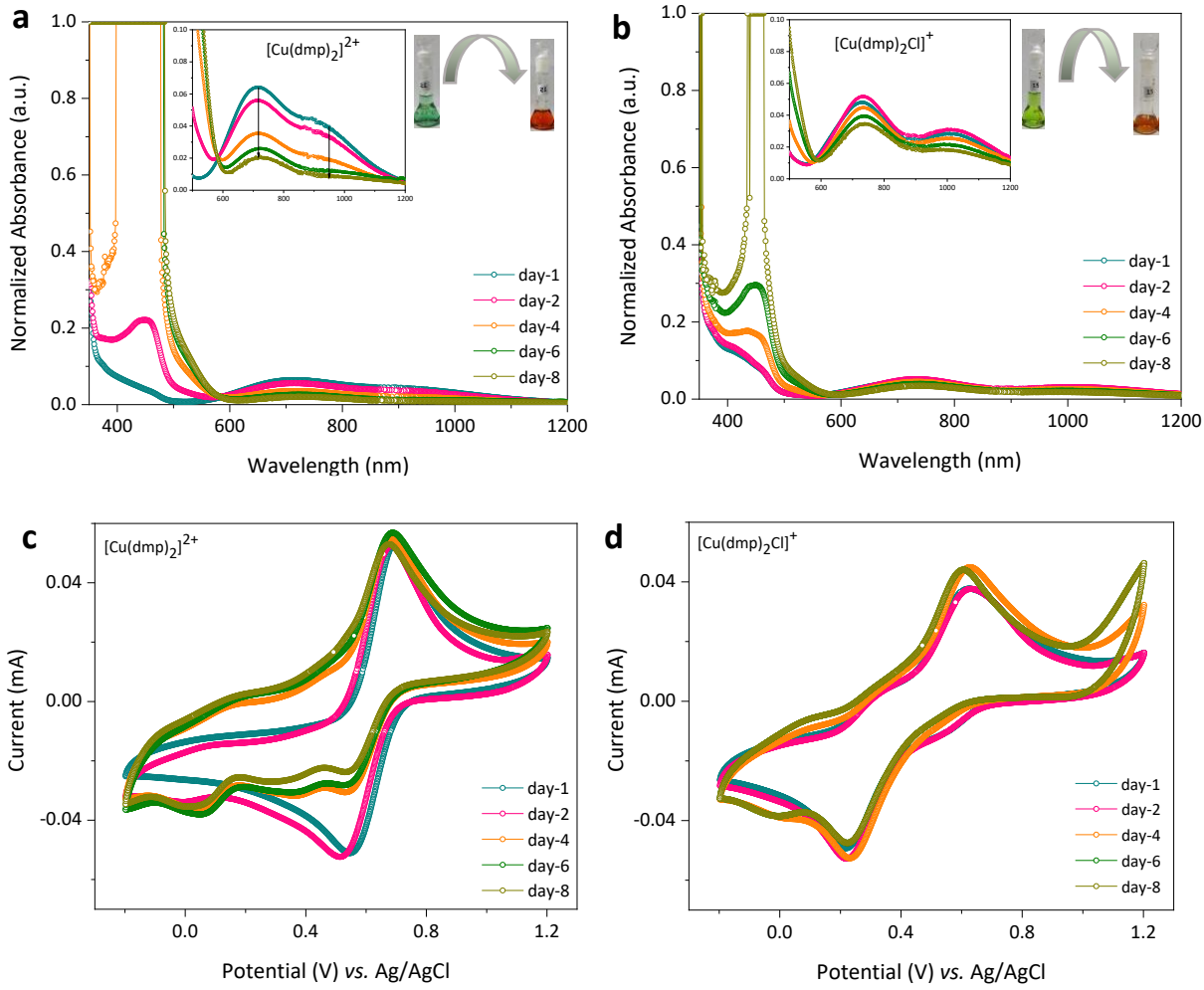

Fig. S7 (a,b) UV-Visible absorption spectra of 3 mM $[Cu(dmp)_2]^{2+}$ and $[Cu(dmp)_2Cl]^{+}$ in presence of 15 equivalents of tBP recorded in different days (1-8 days). (c,d) Cyclic voltammogram of 3 mM $[Cu(dmp)_2]^{2+}$ and $[Cu(dmp)_2Cl]^{+}$ in presence of 15 equivalent of tBP and 0.1 M $TBAPF_6$ in acetonitrile solution recorded at 100 mV/s in different days (1-8 days).

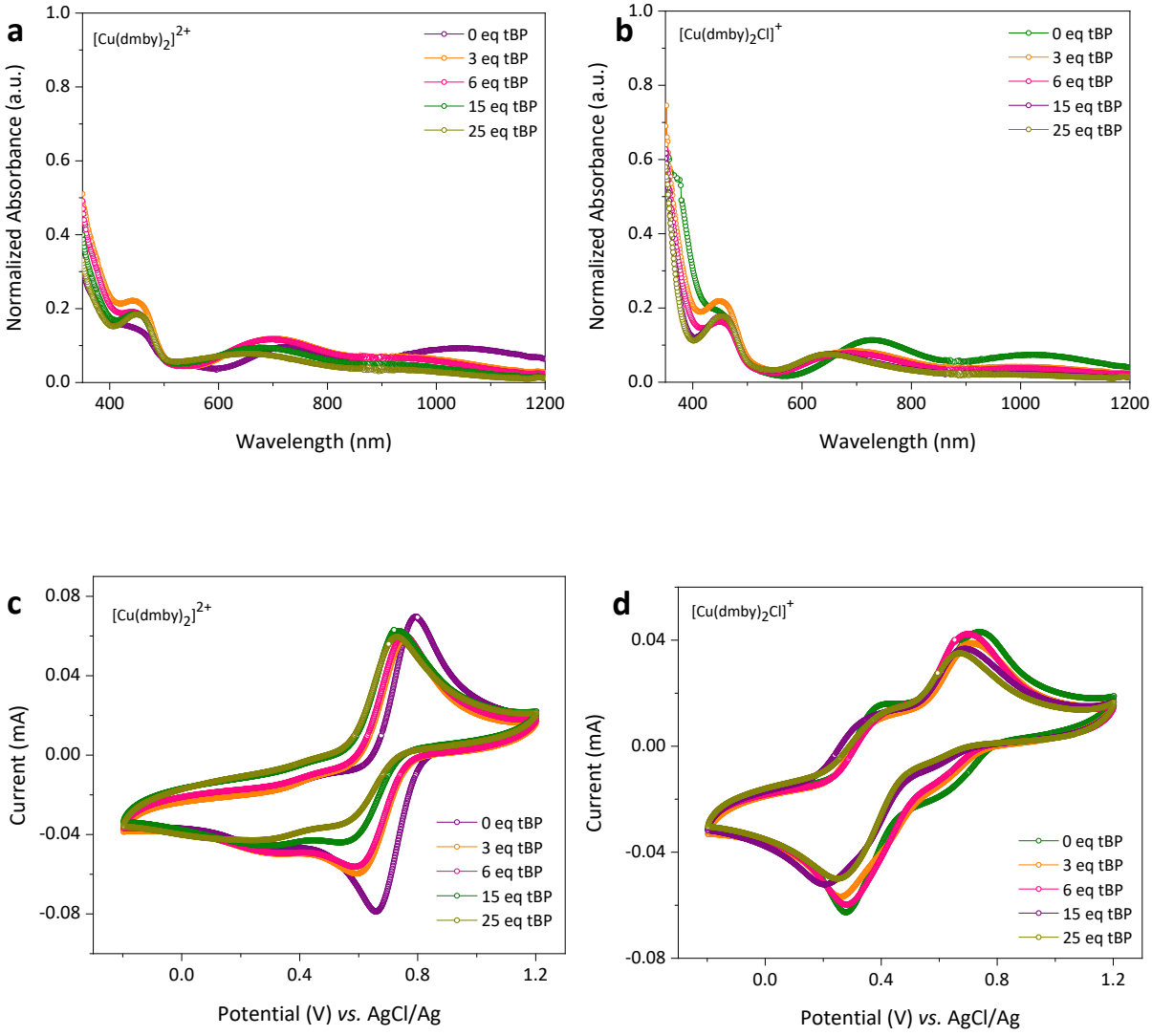

Fig. S8 (a,b) UV-Visible absorption spectra of 3 mM $[Cu(dmby)_2]^{2+}$ and $[Cu(dmby)_2Cl]^{+}$ in presence of different concentrations of tBP (0, 3, 6, 15 and 25 equivalents) in acetonitrile. (c,d) Cyclic voltammogram of 3 mM of $[Cu(dmby)_2]^{2+}$ and $[Cu(dmby)_2Cl]^{+}$ in presence of different concentrations of tBP (0, 3, 6, 15 and 25 equivalents) in 0.1 M $TBAPF_6$/acetonitrile measured at 100mV/s.

^{1}H-NMR spectra of Cu complexes

a

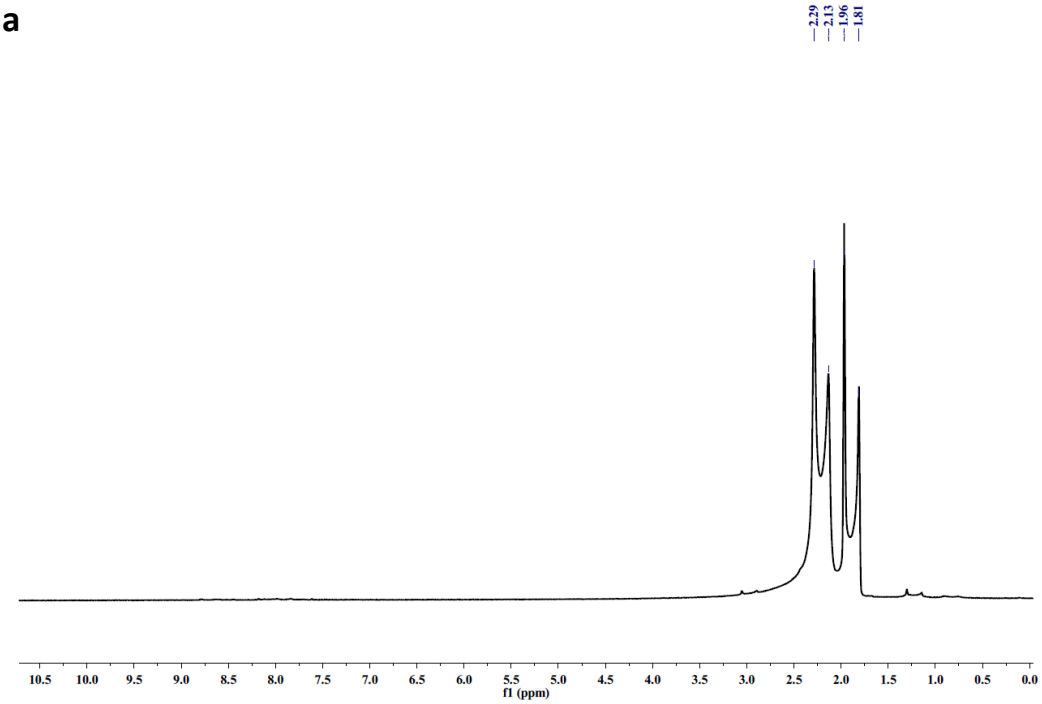

b

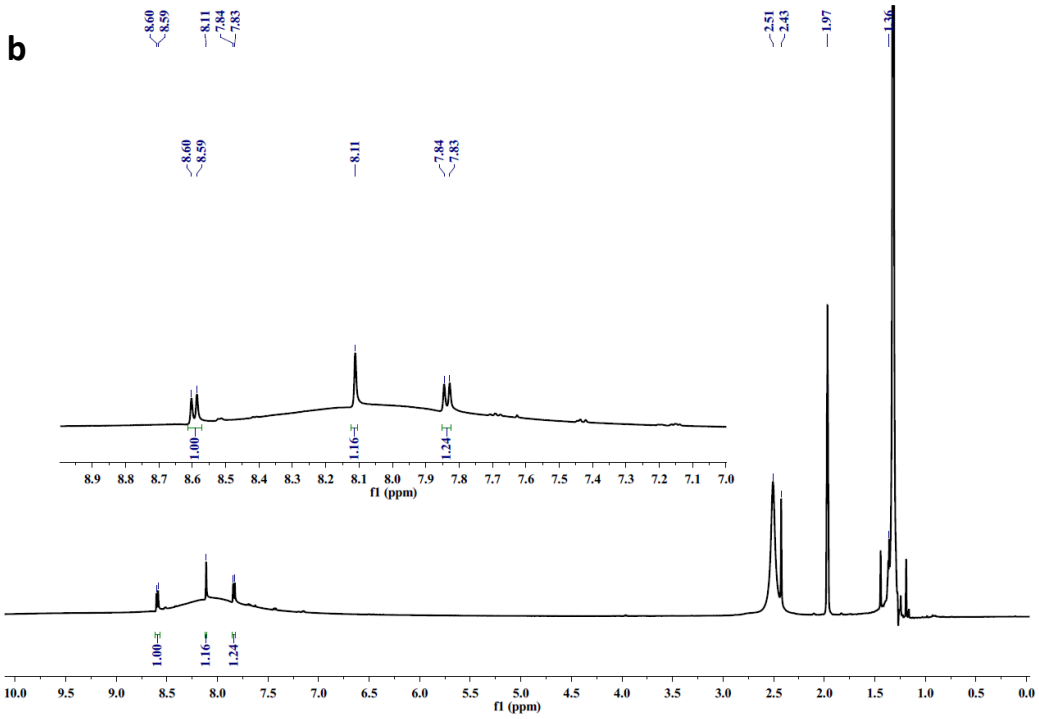

c

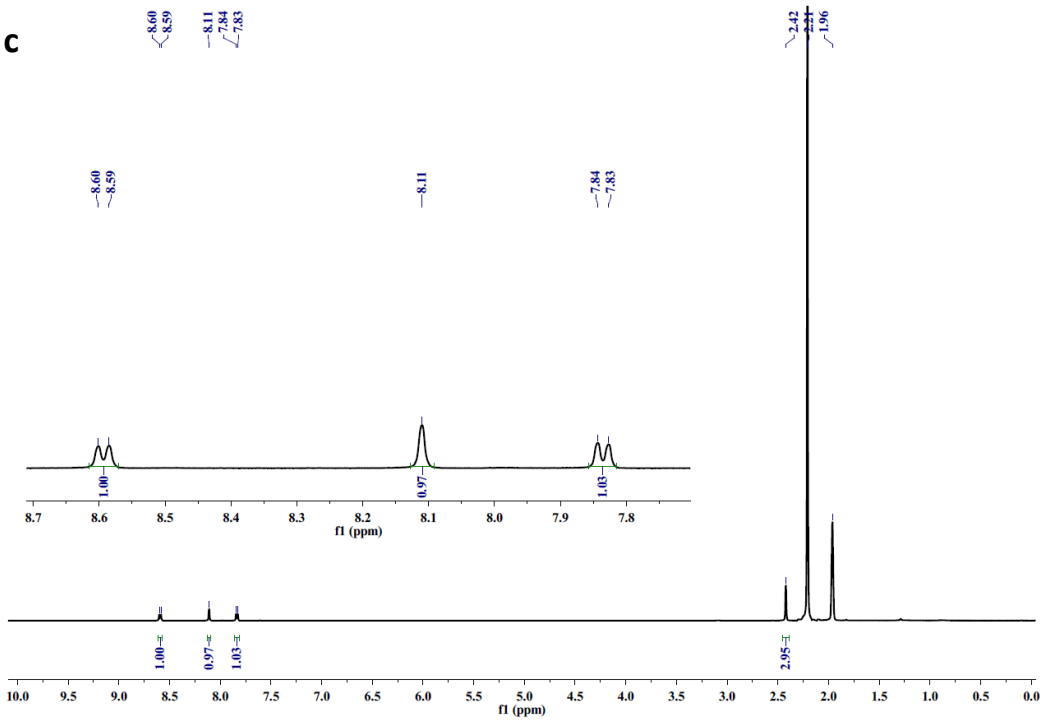
8.60
8.59
8.11
7.84
7.83
2.42
2.21
1.96
1.00
0.97
1.03
2.95
f1 (ppm)

d

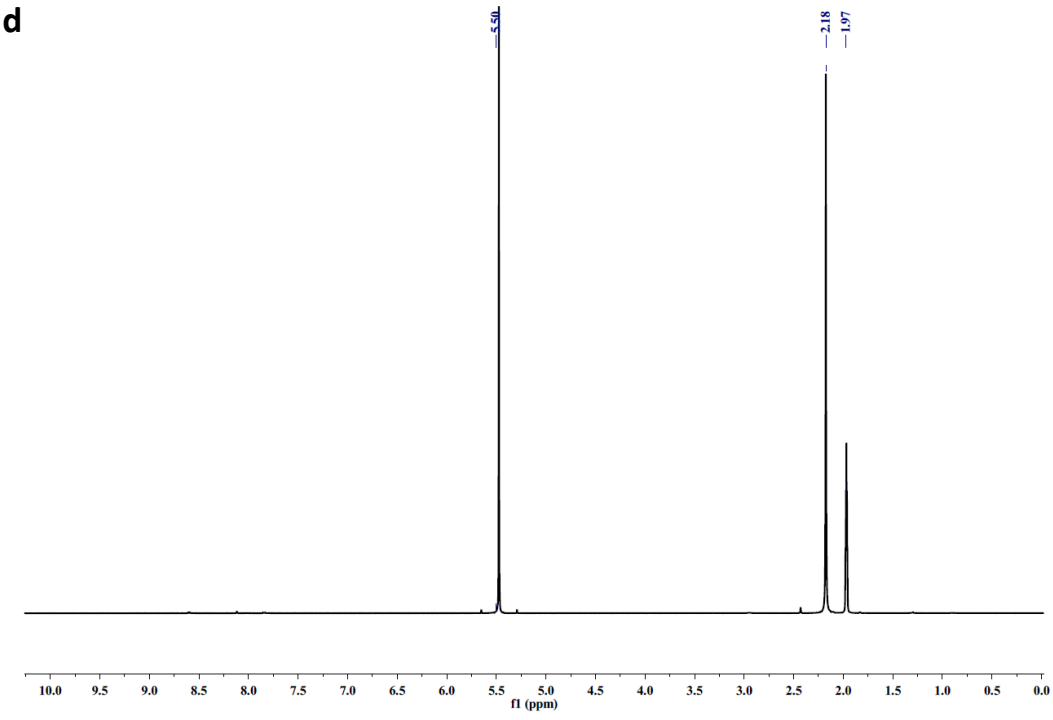
5.50
2.18
1.97
f1 (ppm)

e

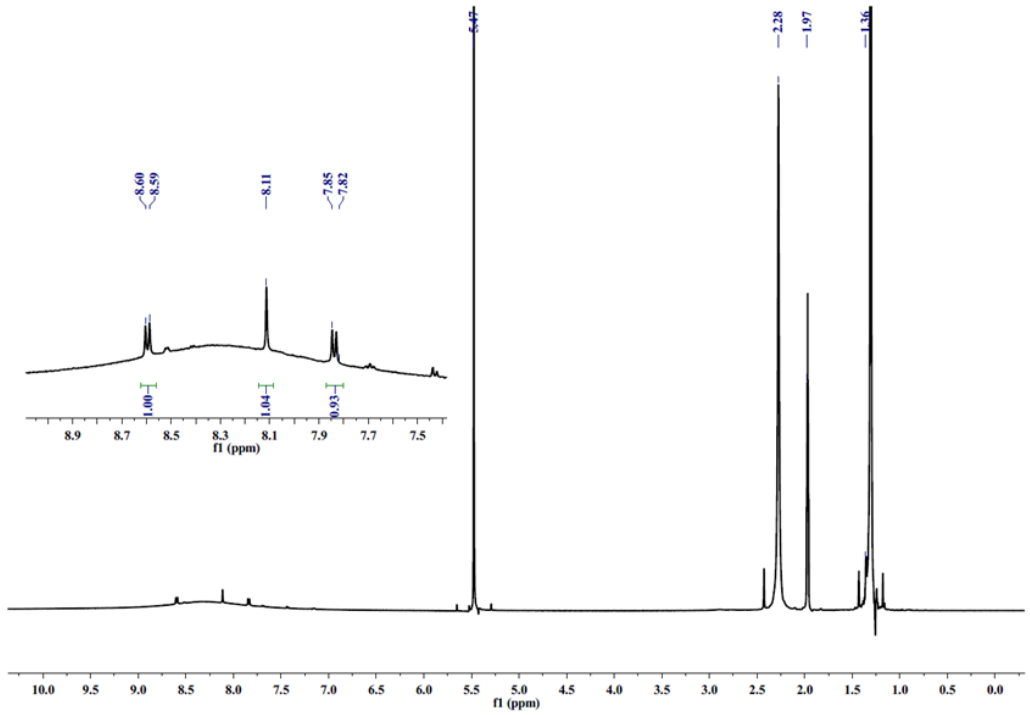
8.60
8.59
8.11
7.85
7.82
5.47
2.28
1.97
1.36
1.00
1.04
0.93
8.9 8.7 8.5 8.3 8.1 7.9 7.7 7.5
f1 (ppm)
10.0 9.5 9.0 8.5 8.0 7.5 7.0 6.5 6.0 5.5 5.0 4.5 4.0 3.5 3.0 2.5 2.0 1.5 1.0 0.5 0.0
f1 (ppm)

f

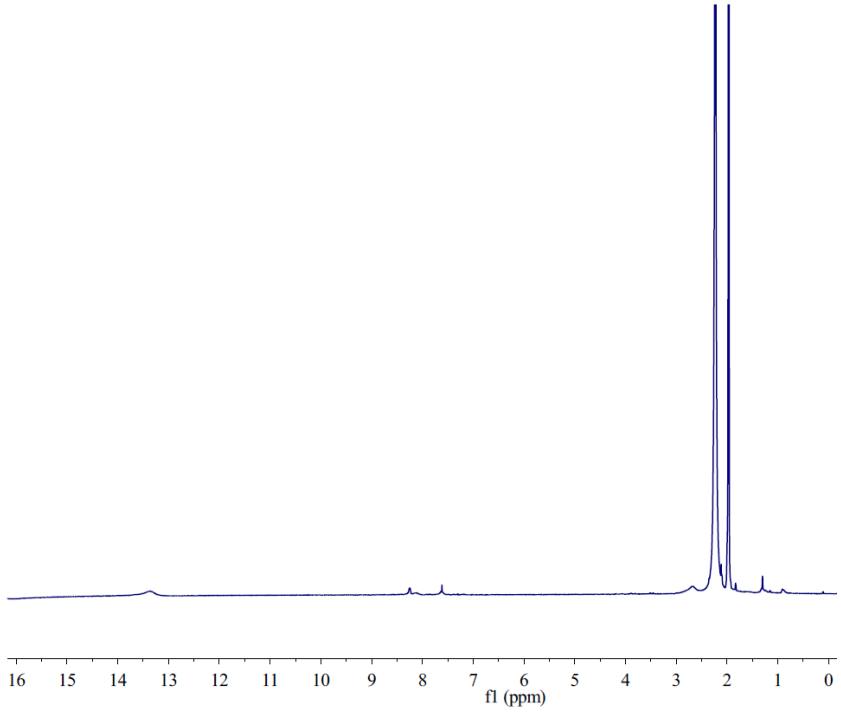
16 15 14 13 12 11 10 9 8 7 6 5 4 3 2 1 0
f1 (ppm)

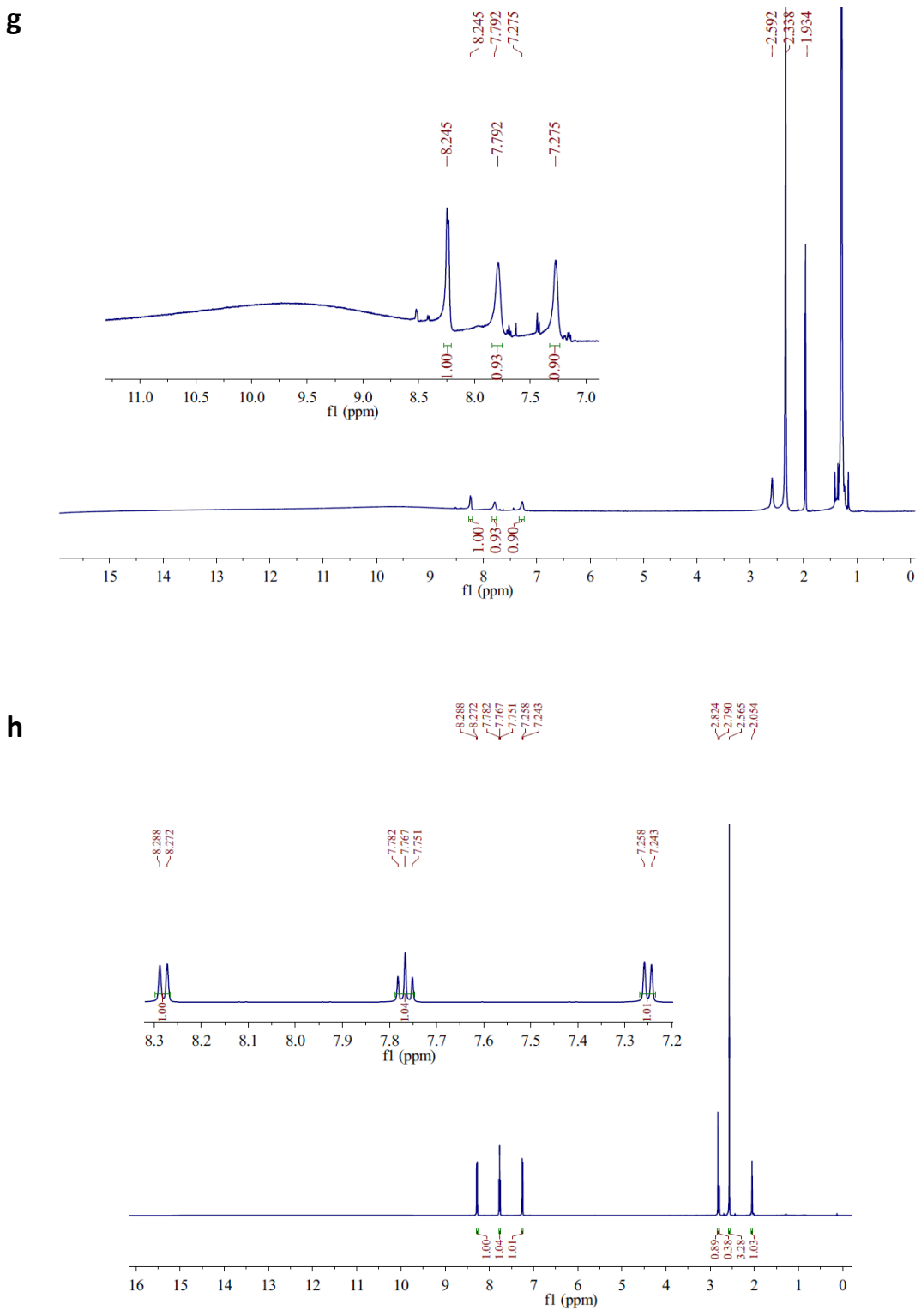

Fig. S9 ^{1}H-NMR spectra of (a) $[Cu(dmp)_2]^{2+}$, (b) $[Cu(dmp)_2]^{2+}$ with 15 equivalents of tBP, (c) $[Cu(dmp)_2]^{+}$, (d) $[Cu(dmp)_2Cl]^{+}$, (e) $[Cu(dmp)_2Cl]^{+}$ with 15 equivalent of tBP, (f) $[Cu(dmby)_2]^{2+}$, (g) $[Cu(dmby)_2]^{2+}$ with 15 equivalents of tBP and (h) free dmby ligand.

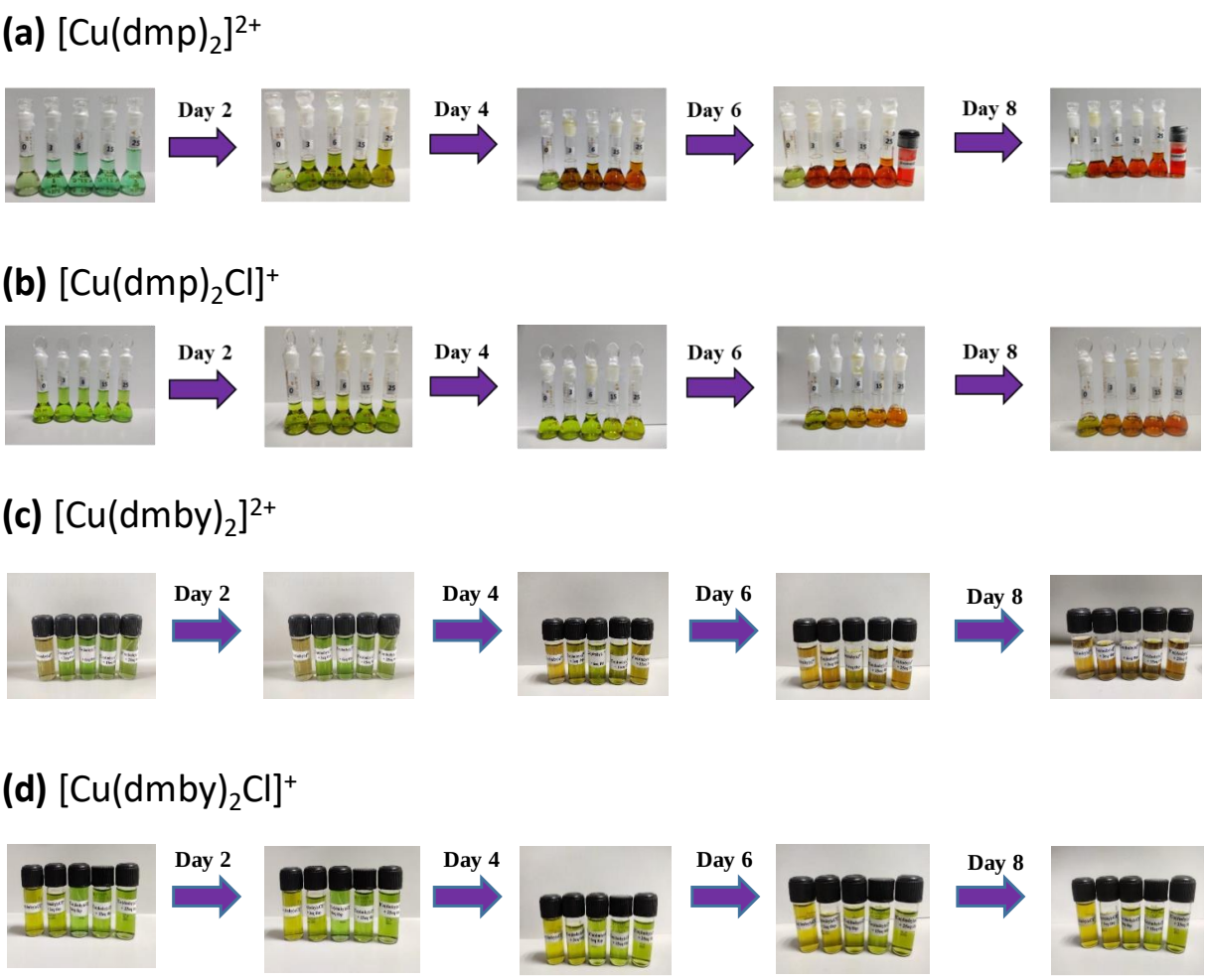

Fig. S10 Change in colour of acetonitrile solution of 3 mM (a)$[Cu(dmp)_2]^{2+}$, (b) $[Cu(dmp)_2Cl]^{+}$, (c) $[Cu(dmby)_2]^{2+}$ and (d) $[Cu(dmby)_2Cl]^{+}$ in presence of different concentration of tBP (0, 3, 6, 15, 25 equivalents) kept at room temperature.

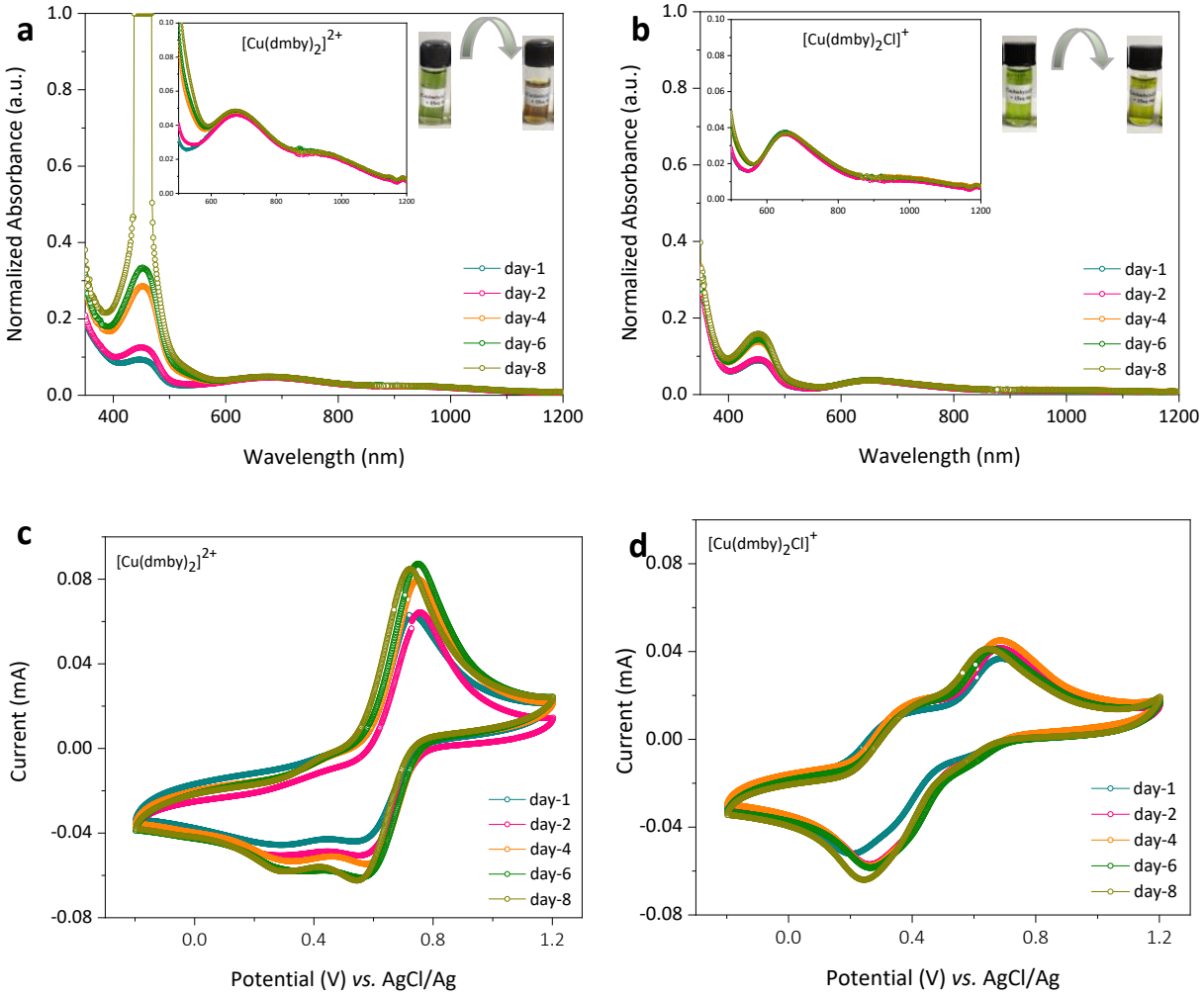

Fig. S11 (a,b) UV-Visible absorption spectra of 3 mM of $[Cu(dmby)_2]^{2+}$ and $[Cu(dmby)_2Cl]^{+}$ in presence of 15 equivalent of tBP recorded at different days (1-8 days). (c,d) Cyclic voltammogram of 3 mM $[Cu(dmby)_2]^{2+}$ and $[Cu(dmby)_2Cl]^{+}$ in presence of 15 equivalent of tBP and 0.1 M $TBAPF_6$ in acetonitrile solution recorded at 100 mV/s in different days (1-8 days).

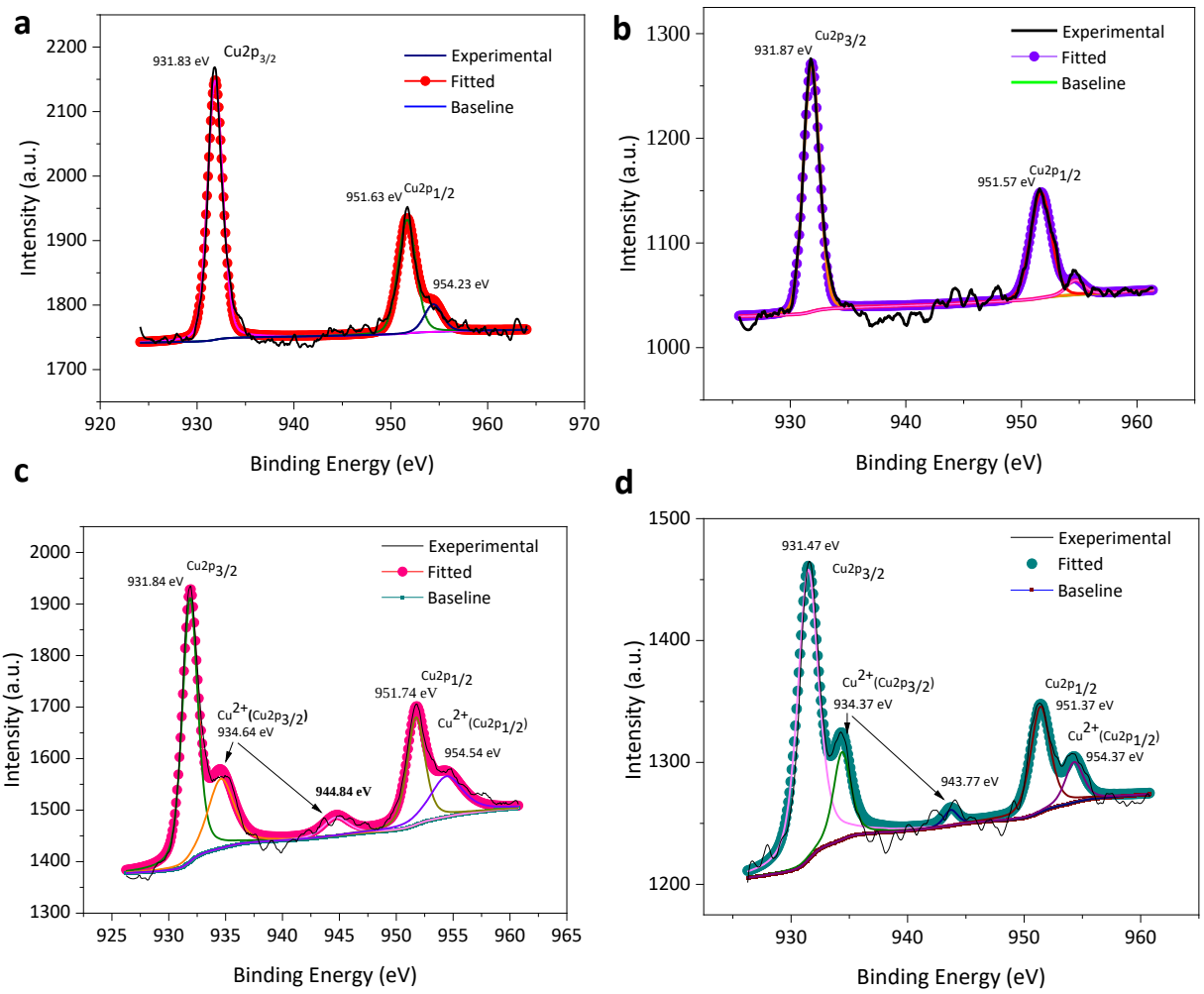

Fig. S12 XPS spectra of (a) $[Cu(dmp)_2]^{2+}$, (b) $[Cu(dmp)_2Cl]^{+}$, (c) $[Cu(dmby)_2]^{2+}$ and (d) $[Cu(dmby)_2Cl]^{+}$ in presence of 15 equivalents of tBP.

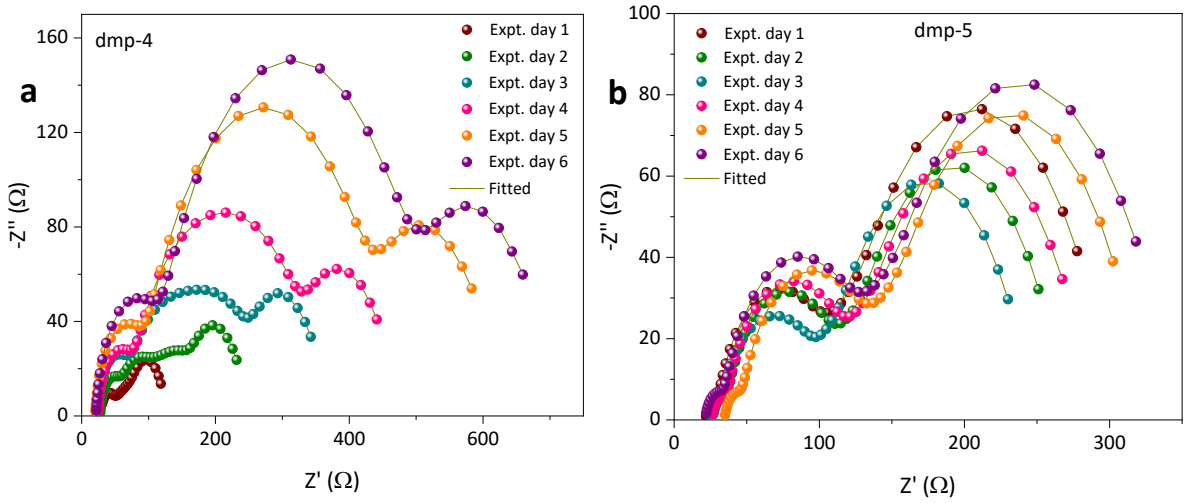

Fig. S13 Evolution of the Nyquist plot of symmetric CE-CE dummy cells for (a) dmp-4 and (b) dmp-5 devices upon ageing under ambient conditions.

The Nyquist plot of CE-CE dummy cell consists of three semicircles, the first semicircle at higher frequency corresponds to the impedance response at the porous electrode, the second and third semicircle corresponds to the impedance response at the PEDOT/electrolyte interface and diffusion of ions in the electrolyte.

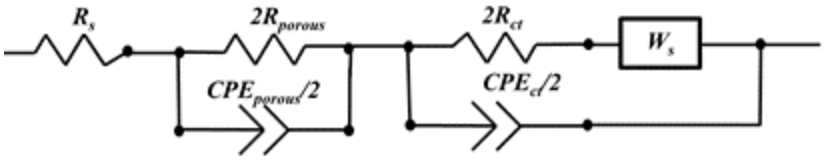

Fig. S14 Equivalent circuit model used for fitting EIS spectra of symmetrical (CE-CE) dummy cells.

The Nyquist plot of CE-CE dummy cell is fitted using the equivalent circuit as shown in Figure S14. It consists of resistance, capacitance and Warburg element. R_s is the series resistance corresponding to resistance due to FTO and the contacts. R_{porous} and CPE_{porous} are the resistance and capacitance demonstrating charge transfer of electron through porous PEDOT electrode. R_{ct} and CPE_{ct} corresponds to resistance and capacitance demonstrating charge transfer at PEDOT/electrolyte interface. W_s is the Warburg element showing diffusion of ions in electrolyte.

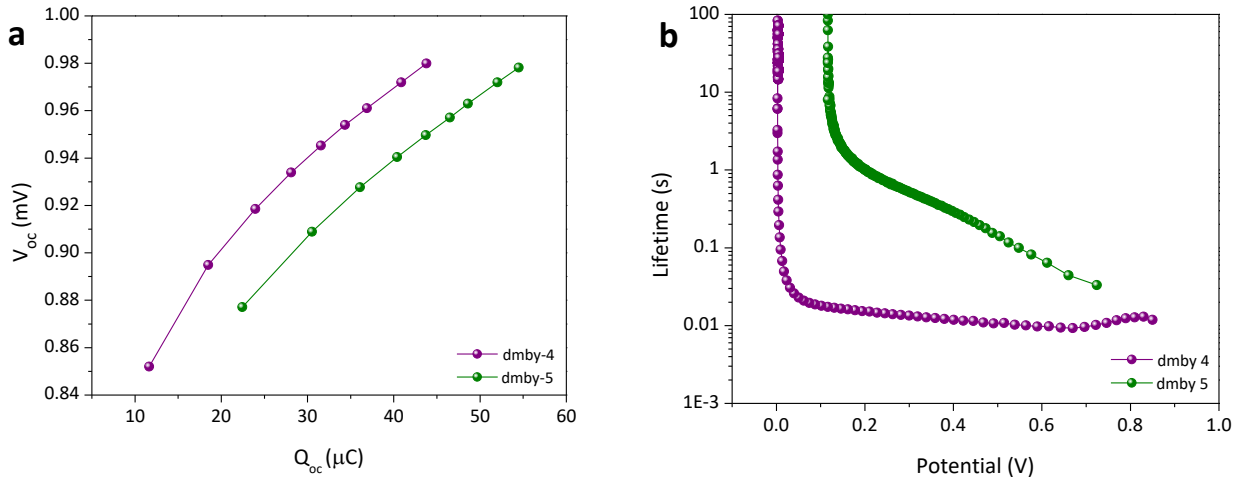

Fig. S15 (a) Plot of extracted charge as function of V_{oc} and (b) lifetime measurement from open circuit voltage decay for dmby-4 and dmby-5 electrolyte-based DSCs using Y123 sensitizer.

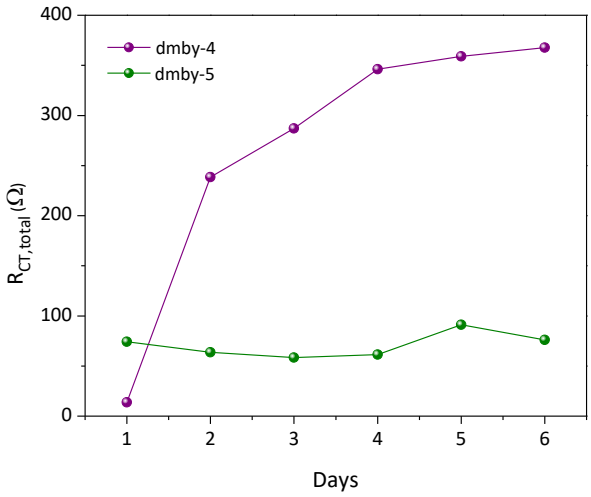

Fig. S16 $R_{CT,total}$ *vs* time for dmby-4 and dmby-5 derived from symmetric CE-CE dummy cell measurements. Y123 was used as the sensitizer in all devices.

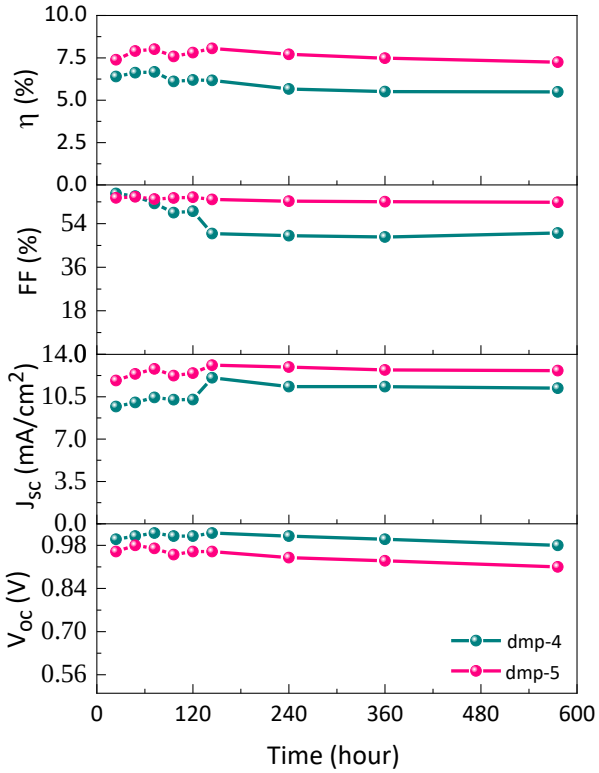

Fig. S17 Evolution of the cell characteristics upon continuous 1 sun (100 mW/cm^2) light soaking of Y123-based DSCs including either dmp-4 or dmp-5-based electrolyte.

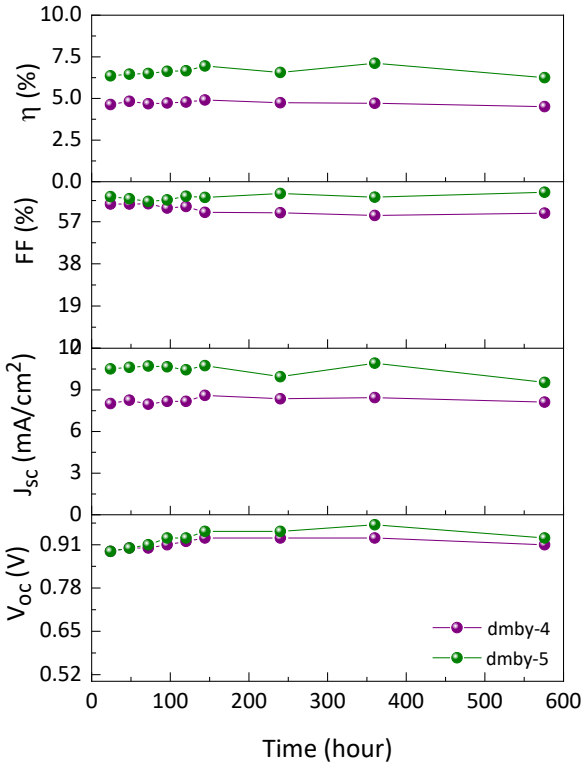

Fig. S18 Evolution of the cell characteristics upon continuous 1 sun (100 mW/cm^2) light soaking of Y123-based DSCs including either dmby-4 or dmby-5-based electrolyte.

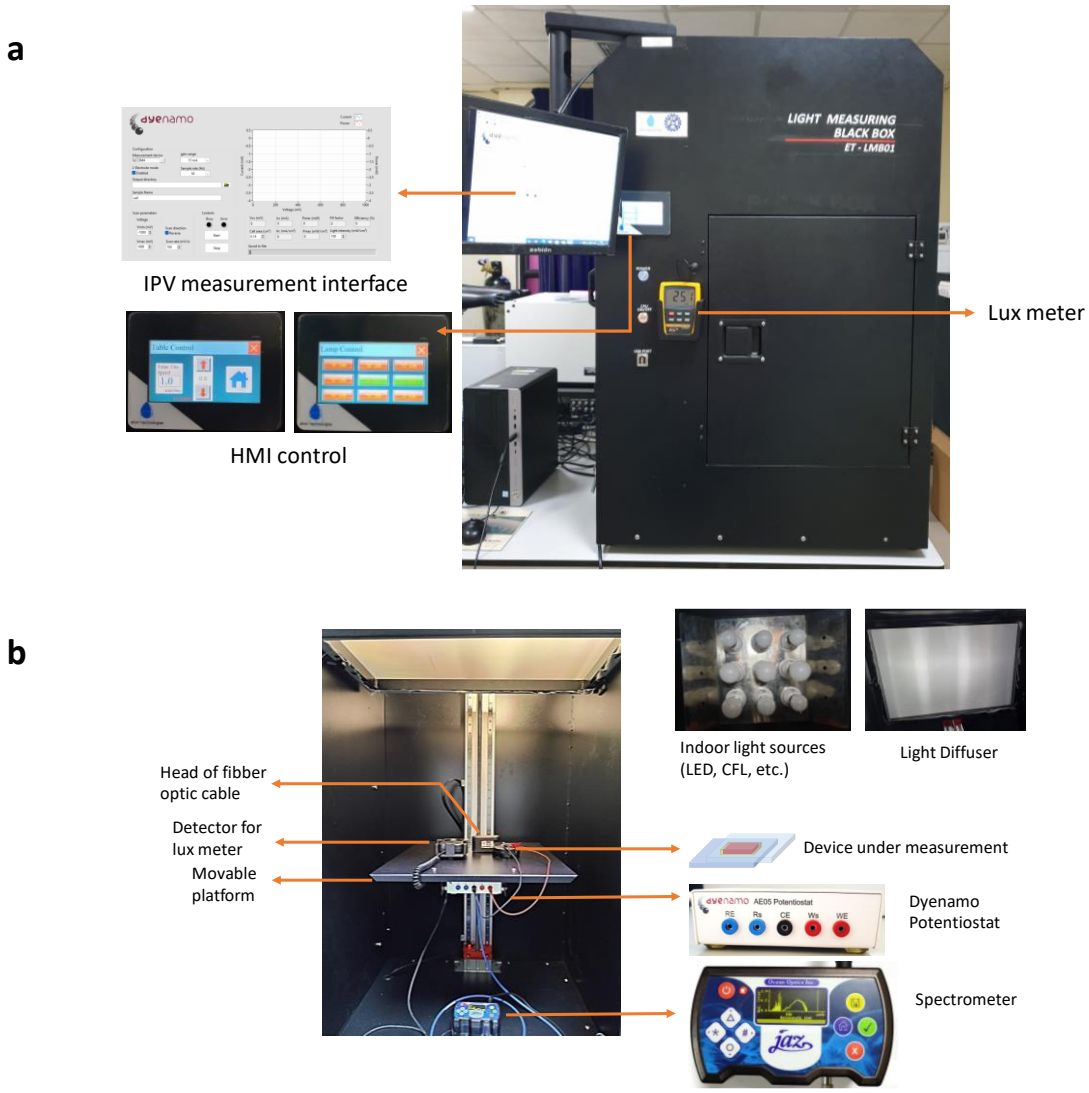

Fig. S19 (a) Outside view and (b) inside view of the custom designed indoor photovoltaic measuring setup integrated with optical fiber spectrometer, lux meter and potentiostat.

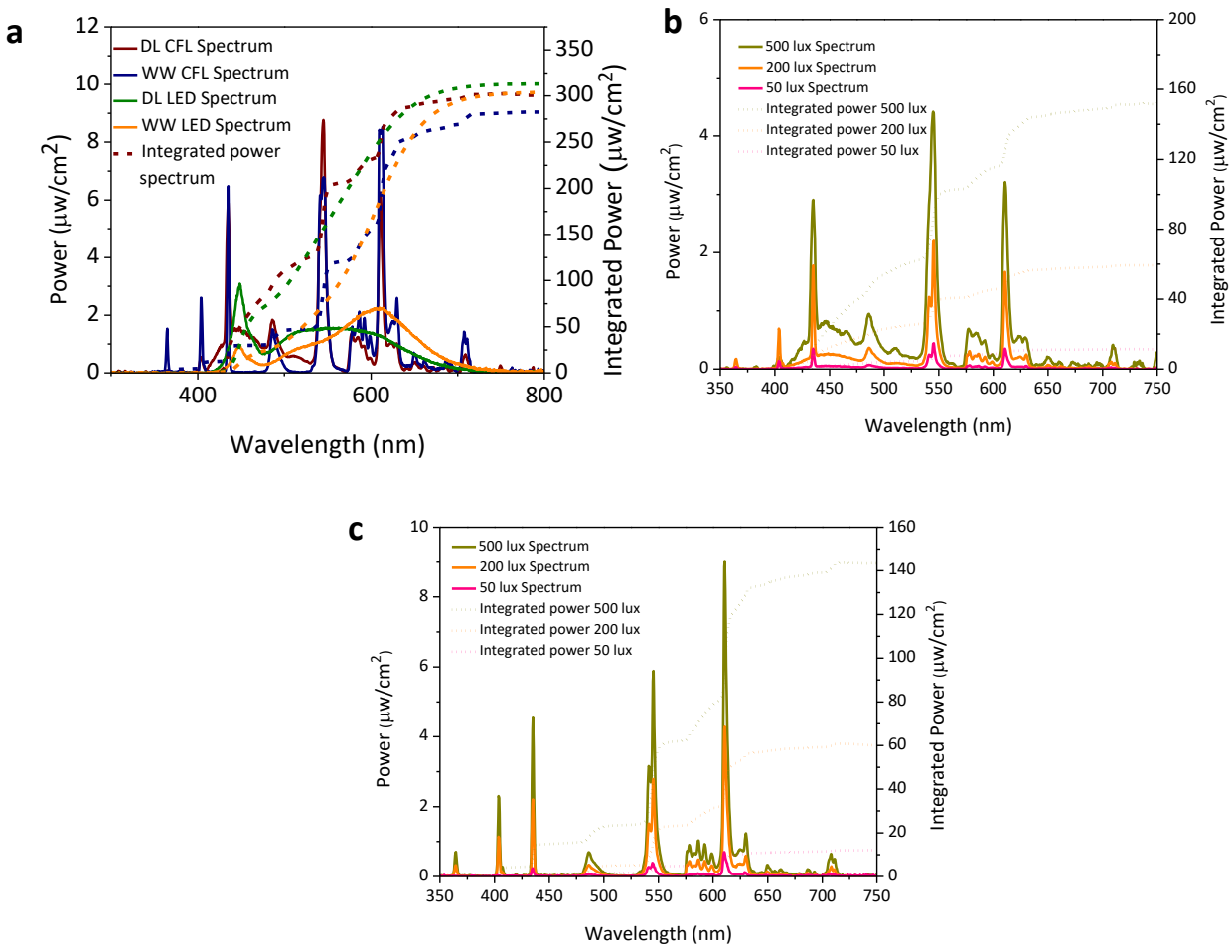

Fig. S20 (a) Power spectra and integrated power in µW/cm^2 for four different indoor illumination sources, daylight CFL (DL CFL), warm white CFL (WW CFL), daylight LED (DL LED), warm white LED (WW LED) under 1000 lux illumination. (b) Power spectra and integrated power in µW/cm^2 for Osram day light fluorescent (DL CFL) illumination at 500 lux, 200 lux and 50 lux. (c) Power spectra and integrated power in µW/cm^2 for Osram warm white fluorescent (WW CFL) illumination at 500 lux, 200 lux and 50 lux

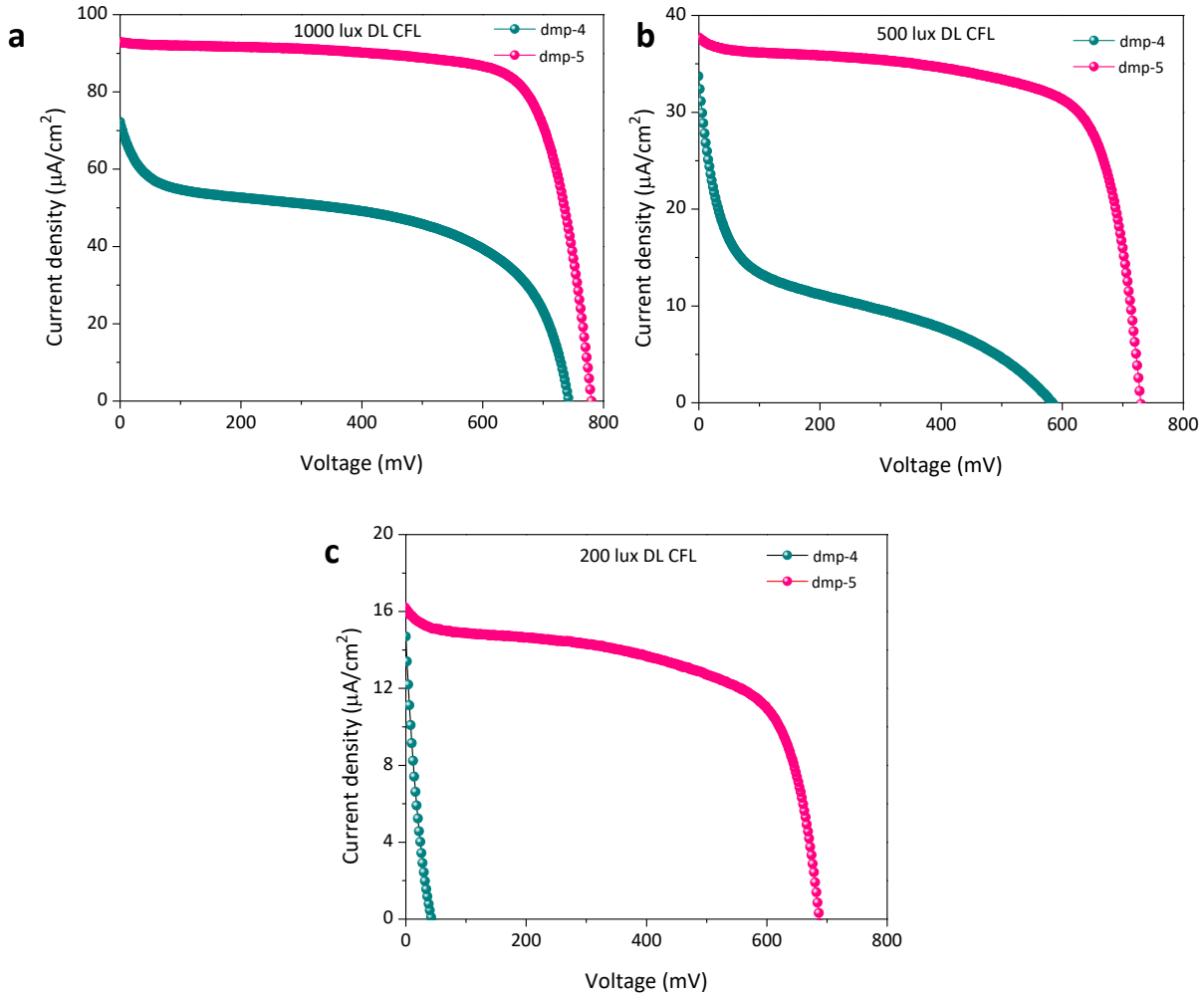

Fig. S21 *J-V* curves for Y123 sensitized DSCs consisting of dmp-4 and dmp-5 electrolytes measured under (a) 1000 lux, (b) 500 lux and (c) 200 lux day light CFL illumination.

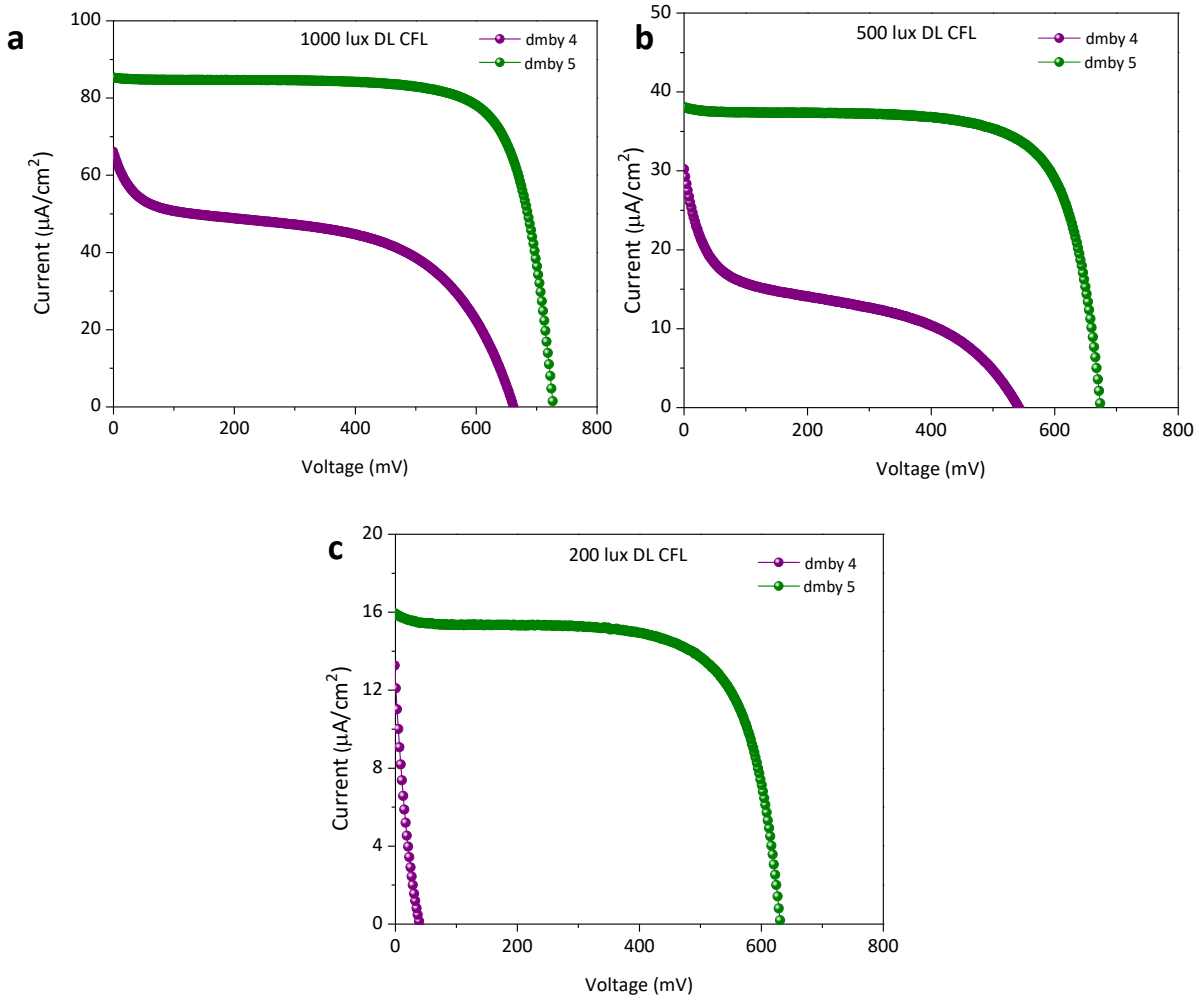

Fig. S22 *J-V* curves for Y123 sensitized DSCs consisting of dmby-4 and dmby-5 electrolytes measured under (a) 1000 lux, (b) 500 lux and (c) 200 lux day light CFL illumination.

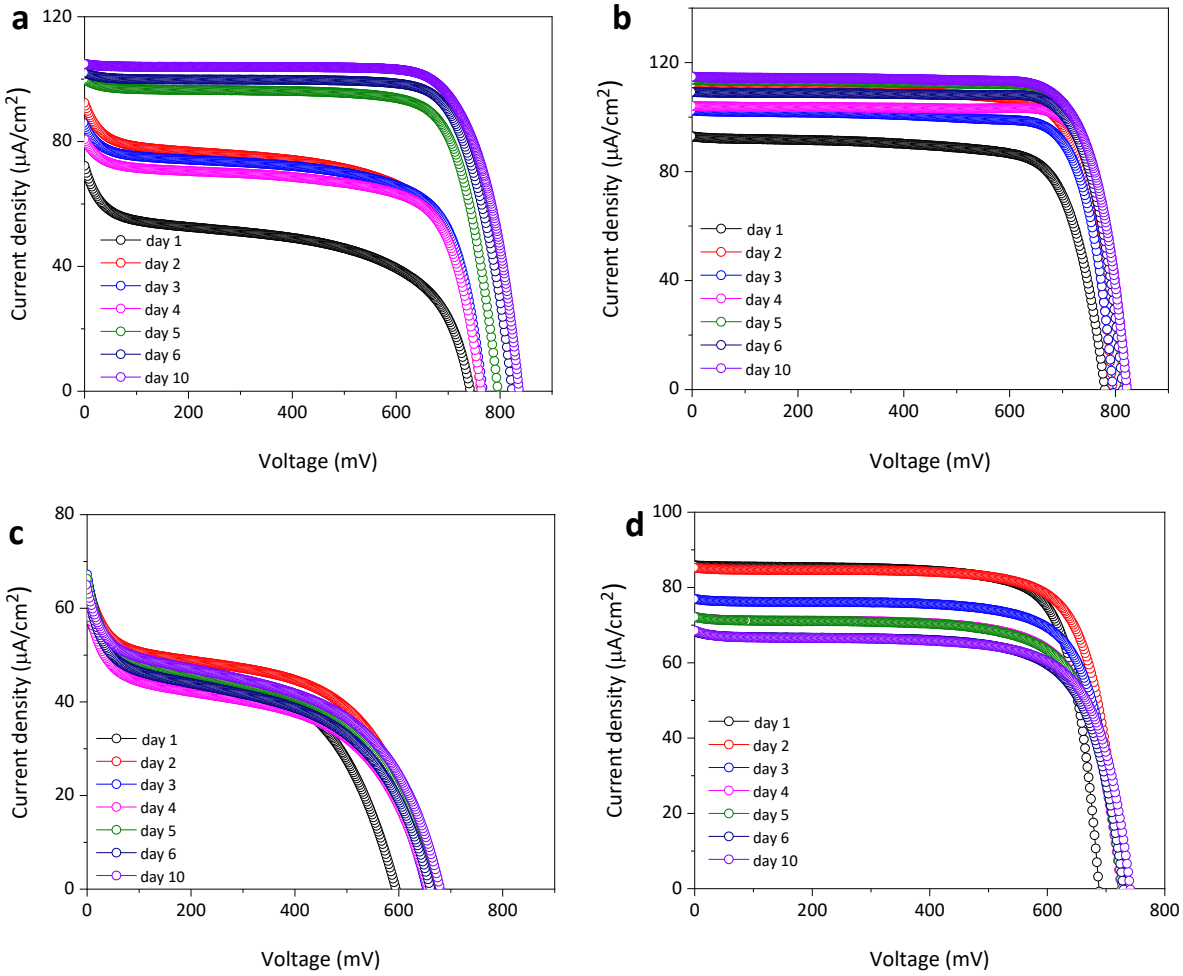

Fig. S23 *J-V* curves for Y123 sensitized DSCs consisting of (a) dmp-4, (b) dmp-5, (c) dmby-4 and (d) dmby-5 electrolytes under 1000 lux day light CFL illumination for 10 days.

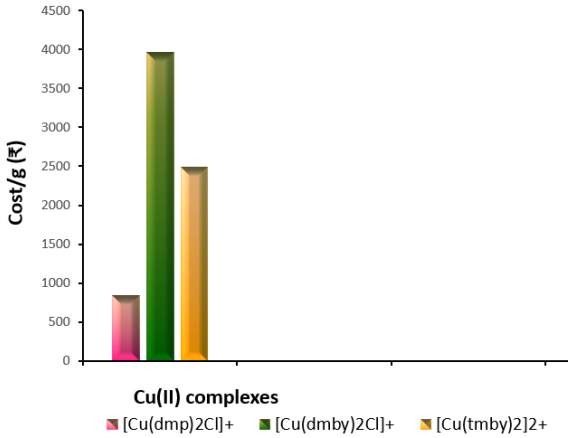

Fig. S24 Graphical representation of the approximate calculated cost/g values for the synthesis of oxidized Cu(II) complexes, $[Cu(dmp)_2Cl]^+$, $[Cu(dmby)_2Cl]^+$ and $[Cu(tmby)_2]^{2+}$.

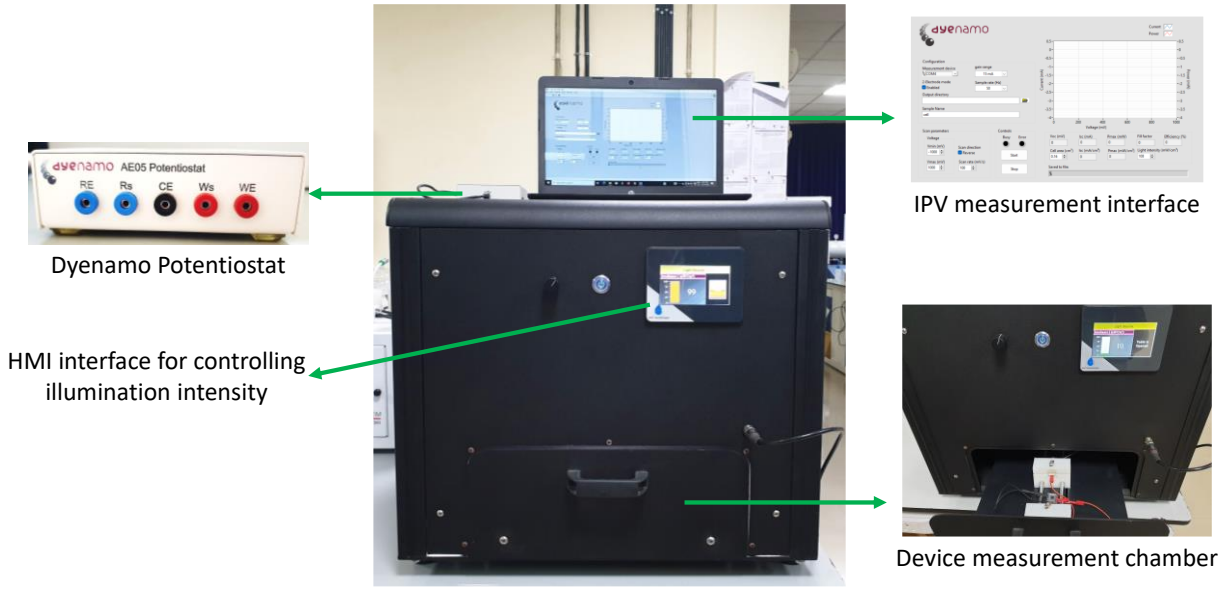

Fig. S25 Custom designed Indoor light soaker used to perform stability measurements.

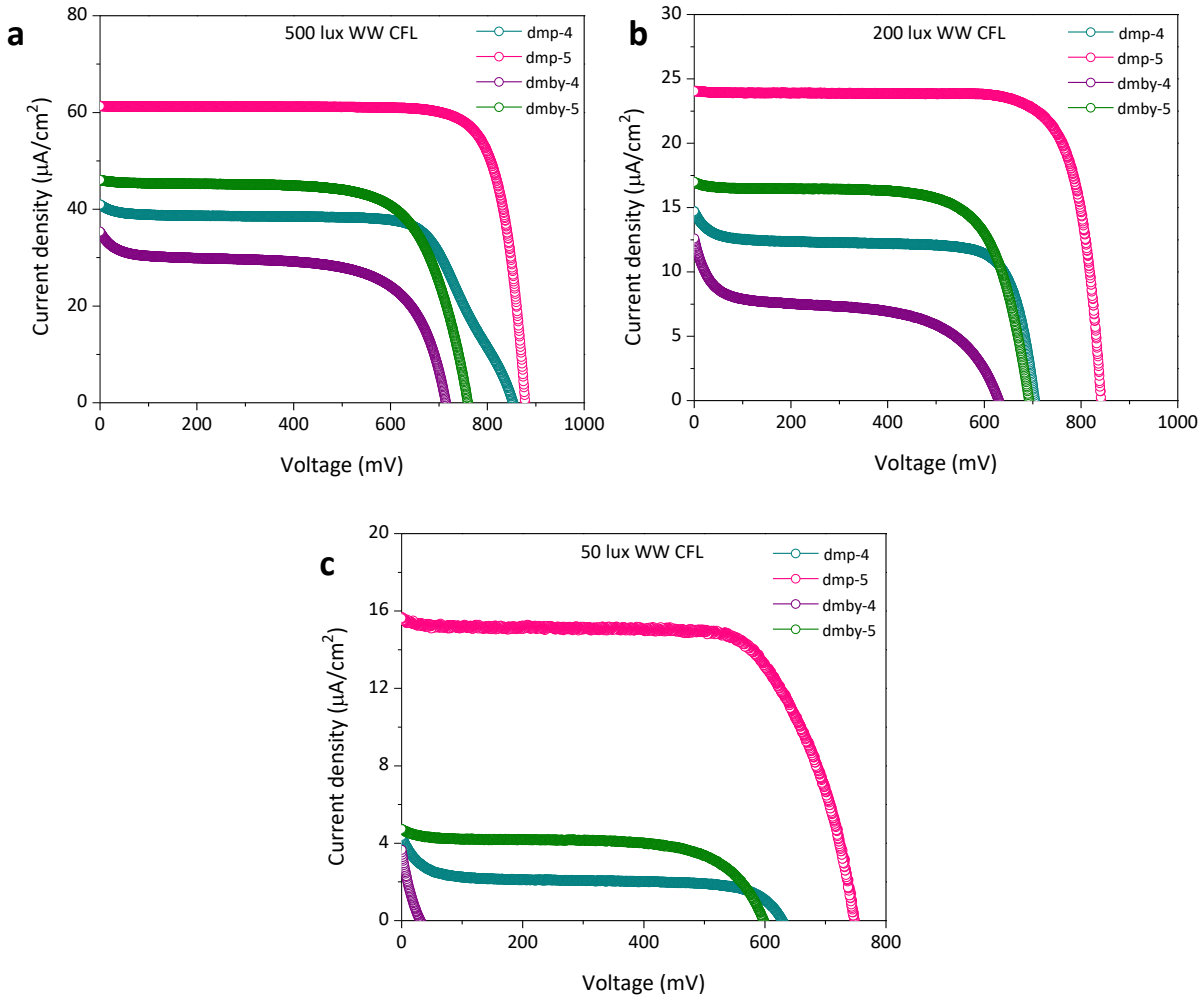

Fig. S26 *J-V* curves for D35:XY1 co-sensitized DSCs fabricated using dmp-4, dmp-5, dmby-4 and dmby-5 electrolytes measured under (a) 500 lux, (b) 200 lux and (c) 50 lux warm white CFL illumination.

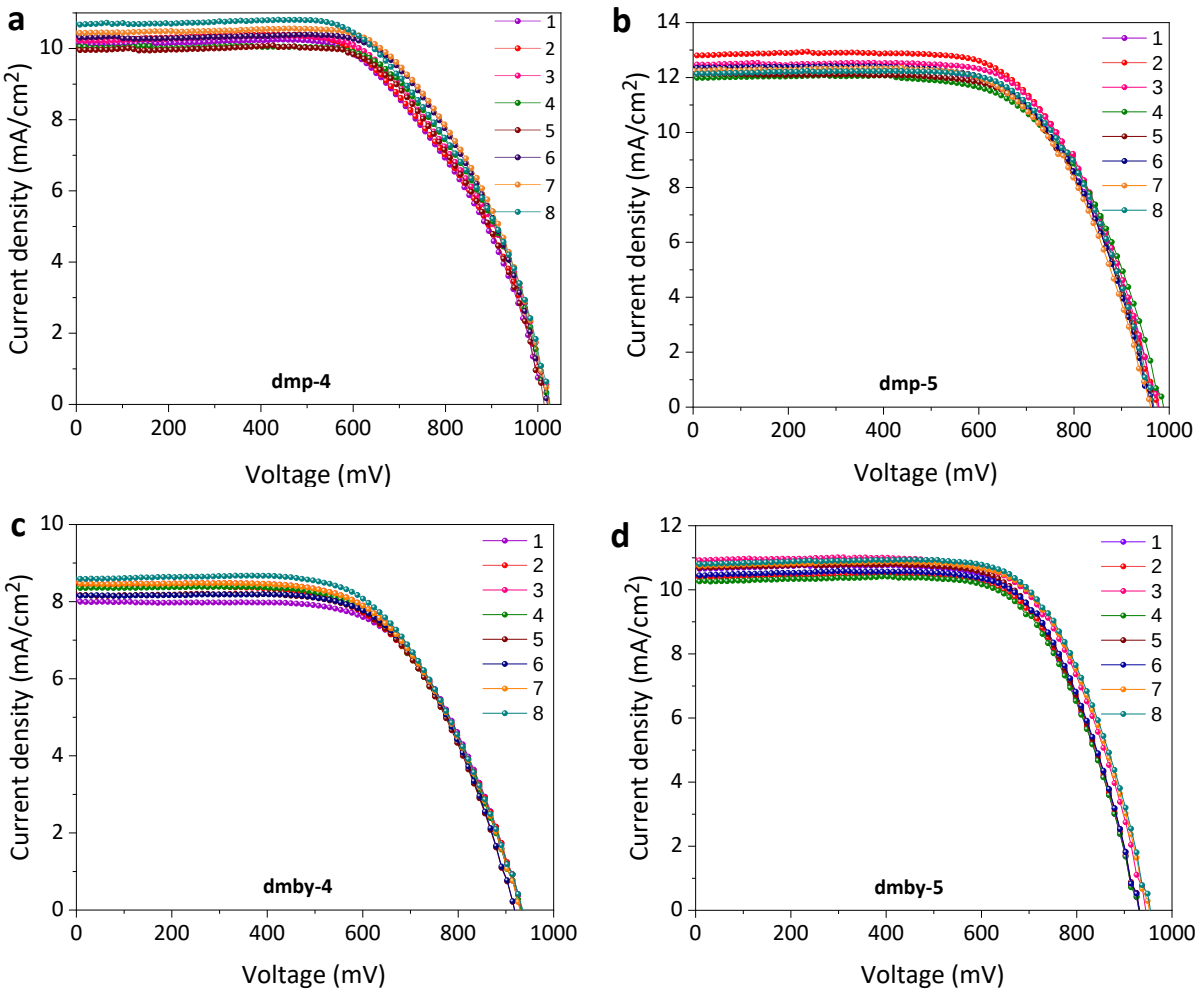

Fig. S27 J-V characteristics of all devices used to calculate error as given in Table 1.

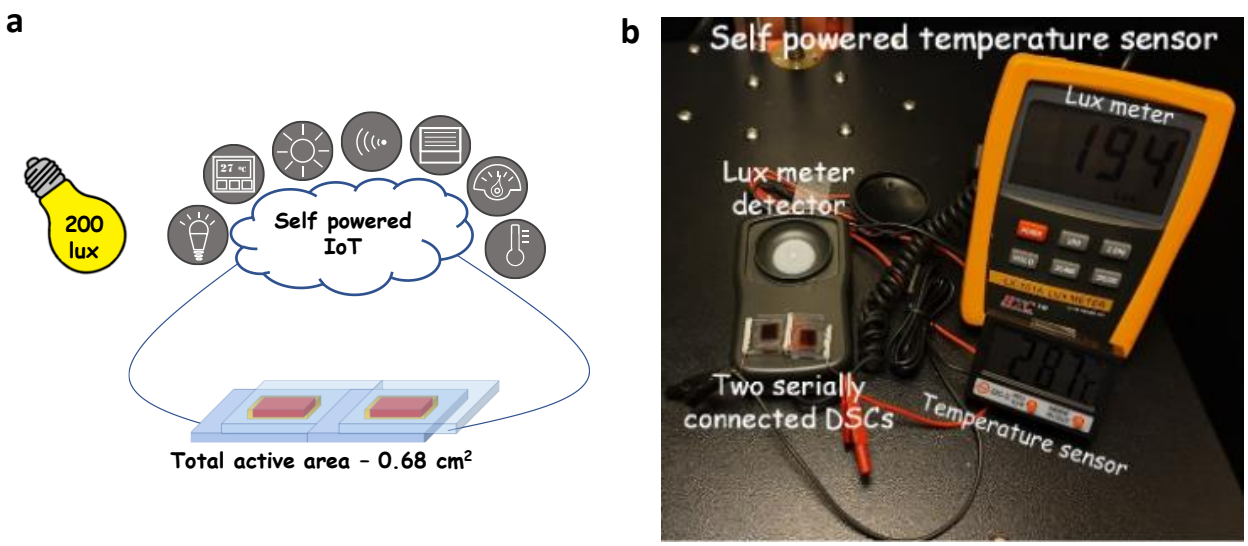

Fig. S28 (a) Illustrative representation of self-powered IoT using DSCs. (b) Image of self-powered temperature sensor powered using two serially connected D35:XY1 co-sensitized DSCs consisting of dmp-5 electrolyte under 200 lux (warm white fluorescent tube) illumination.

Fig. S29 Semi-automated dye-sensitized solar cell/module fabrication facility used for the fabrication of DSCs in multiple batches.

Table S1 Tabulated integrated power in μW/cm^2 for day light CFL (DL CFL), warm white CFL (WW CFL), day light LED (DL LED) and warm white LED (WW LED) under different light intensities (1000, 500, 200 and 50 lux).

Light Sources	Intensity (lux)	Integrated Power (μW/cm^2)
day light CFL (DL CFL)	1000	306.6
	500	152.7
	200	58.0
	50	10.2
warm white CFL (WW CFL)	1000	283.4
	500	143.1
	200	59.1
	50	12.0
day light LED (DL LED)	1000	312.8
warm white LED (WW LED)	1000	303.2

Table S2 Bond length (Å) and angles (deg) for $[Cu(dmp)_2Cl]^+$ and $[Cu(dmp)Cl_2tBP]$ complexes obtained from single crystal X-ray diffraction.

$[Cu(dmp)_2Cl]^+$		**$[Cu(dmp)Cl_2tBP]$**	
Cu-N1	2.174	Cu-N1	2.271
Cu-N2	2.018	Cu-N2	2.013
Cu-N3	2.102	Cu-N3	2.025
Cu-N4	2.015	Cu-Cl1	2.325
Cu-Cl	2.325	Cu-Cl2	2.309
N1-Cu-Cl1	114.43	Cl2-Cu-Cl1	156.90
N2-Cu-Cl1	84.79	N1-Cu-Cl1	101.43
N3-Cu-Cl1	137.76	N2-Cu-Cl1	85.63
N4-Cu-Cl1	90.08	N3-Cu-Cl1	89.64
N2-Cu-N1	79.9	N1-Cu- Cl2	99.49
N2-Cu-N3	99.6	N2-Cu- Cl2	89.10
N3-Cu-N1	107.7	N3-Cu- Cl2	93.52
N4-Cu-N1	107.2	N2-Cu-N1	78.33
N4-Cu-N2	172.6	N2-Cu-N3	173.44
N4-Cu-N3	80.6	N3-Cu-N1	107.11

Table S3 Formal redox potential of four coordinated and five coordinated copper complexes without tBP and with 15 equivalent of tBP in presence of 0.1M $TBAPF_6$ as supporting electrolyte in acetonitrile solution (3mM) calculated in V *vs.* NHE. The $E_{1/2}$ of ferrocene redox couple was taken as 0.395 V *vs.* NHE.

Copper complexes	**Redox potential (V *vs.* NHE)**
$[Cu(dmp)_2]^{2+/+}$	0.93
$[Cu(dmp)_2]^{2+}$ + 15 tBP	0.85
$[Cu(dmp)_2Cl]^{+}$	0.69
$[Cu(dmp)_2Cl]^{+}$ + 15 tBP	0.65
$[Cu(dmby)_2]^{2+/+}$	0.95
$[Cu(dmby)_2]^{2+}$ + 15 tBP	0.87
$[Cu(dmby)_2Cl]^{+}$	0.73
$[Cu(dmby)_2Cl]^{+}$ + 15 tBP	0.67

Table S4 The tabulated $R_{CT, total}$ (Ω) measured using EIS of dummy cells for dmp-4, dmp-5, dmby-4 and dmby-5 electrolytes under dark condition at zero volt for different days.

Days	$R_{CT, total}$ (Ω)			
	dmp-4	**dmp-5**	**dmby-4**	**dmby-5**
day 1	81	103	213.8	74.3
day 2	161.1	109.3	238.4	63.6
day 3	261	95.5	287	58.4
day 4	340.3	115.6	346.2	61.4
day 5	448.2	131.2	359.1	91.1
day 6	516.2	126.2	367.7	76.1

Table S5 The *J-V* characteristics of Y123 sensitized dmp-4 and dmp-5 electrolyte based devices under various illumination intensities (1000 lux, 500 lux and 200 lux) using day light CFL.

Input Power ($\mu W/cm^2$)	**Electrolyte**	**V_{oc} (mV)**	**J_{sc} ($\mu A/cm^2$)**	**FF (%)**	**η (%)**	**Output Power ($\mu W/cm^2$)**	**% increase in efficiency (%)**
1000 lux (306.59)	dmp-4	741.9 ± 2.7	72.2 ± 0.5	44.5 ± 0.4	7.8 ± 0.2	23.9	
	dmp-5	780.2 ± 0.6	98.7 ± 2.1	74.8 ± 0.1	18.8 ± 0.4	57.6	58.6
500 lux (152.67)	dmp-4	583.4 ± 3.	33.7 ± 0.2	15.8 ± 0.2	2.04 ± 0.1	3.1	
	dmp-5	730 ± 1.5	37.7 ± 0.1	68.6 ± 0.3	12.4 ± 0.1	18.9	83.5
200 lux (58.04)	dmp-4	42 ± 0.7	14.7 ± 0.4	17.3 ± 0.1	0.2 ± 0.1	0.1	
	dmp-5	688.4 ± 0.4	16.1 ± 0.1	60.4 ± 0.1	11.6 ± 0.1	6.7	98.4

Table S6 Photovoltaic parameters of Y123 sensitized dmp-4 and dmp-5 electrolyte based devices under 1000 lux (306.59 μW/cm^2) day light CFL illumination for 10 days.

Time	Electrolyte	V_{oc} (mV)	J_{sc} (μA/cm^2)	*FF* (%)	Output Power (μW/cm^2)	η (%)
Day 1	dmp-4	741.9 ± 2.7	72.2 ± 0.5	44.5 ± 1.4	23.9	7.8 ± 0.2
	dmp-5	780.2 ± 0.6	98.7 ± 2.1	74.8 ± 0.1	57.6	18.8 ± 0.4
Day 2	dmp-4	763.8 ± 0.6	92.4 ± 0.3	56.7 ± 0.4	40.1	13.1 ± 0.1
	dmp-5	794.3 ± 0.4	112 ± 0.1	77.4 ± 0.1	68.8	22.5 ± 0.1
Day 3	dmp-4	766.1 ± 0.6	85.3 ± 0.2	61.6 ± 0.1	40.3	13.2 ± 0.1
	dmp-5	796.2 ± 0.5	102.4 ± 0.1	79.1 ± 0.1	64.5	21.1 ± 0.1
Day 4	dmp-4	763.9 ± 1.5	80.7 ± 1.4	62.9 ± 0.9	38.8	12.7 ± 0.1
	dmp-5	821 ± 1.9	104.2 ± 0.3	81.3 ± 0.7	69.5	22.7 ± 0.3
Day 5	dmp-4	797 ± 0.8	100 ± 0.1	74.7 ± 0.1	59.9	19.5 ± 0.1
	dmp-5	817.3 ± 0.8	113.8 ± 0.1	79.4 ± 0.1	73.9	24.1 ± 0.1
Day 6	dmp-4	822.8 ± 1.2	102 ± 0.1	76.1 ± 0.1	63.8	20.9 ± 0.1
	dmp-5	814.0 ± 0.5	109.2 ± 0.1	80.1 ± 0.1	71.2	23.6 ± 0.1
Day 10	dmp-4	836.2 ± 3.6	104.9 ±0.2	76.3 ± 1.0	66.9	21.9 ± 0.4
	dmp-5	821.3 ± 1.4	114.9 ± 0.1	78.6 ± 0.5	74.1	24.2 ± 0.2

Table S7 *J-V* characteristics of Y123 sensitized dmby-4 and dmby-5 devices under 1000 lux, 500 lux and 200 lux day light CFL illumination.

Input Power ($\mu W/cm^2$)	**Electrolyte**	**V_{oc} (mV)**	**J_{sc} ($\mu A/cm^2$)**	***FF* (%)**	**Output Power ($\mu W/cm^2$)**	**η (%)**	**% increase in efficiency (%)**
1000 lux (306.59)	dmby-4	661.8 ± 4.6	66.1 ± 1.1	44.3 ± 0.4	19.4	6.3 ± 0.2	58.8
	dmby-5	726.7 ± 2.5	85.3 ± 1.5	75.8 ± 1	47	15.3 ± 0.1	
500 lux (152.67)	dmby-4	541.9 ± 2.6	30.2 ± 0.1	25.6 ± 0.6	4.2	2.8 ± 0.1	77.2
	dmby-5	673.8 ± 0.6	38.1 ± 0.1	71.9 ± 0.1	18.4	12.1 ± 0.1	
200 lux (58.04)	dmby-4	40.7 ± 0.3	12.1 ± 0.1	17.6 ± 0.1	0.1	0.1 ± 0.1	98.8
	dmby-5	630.7 ± 0.8	15.9 ± 0.2	68.4 ± 1.6	6.9	11.8 ± 0.2	

Table S8 Photovoltaic parameters of Y123 sensitized DSCs using dmby-4 and dmby-5 electrolytes under 1000 lux day light CFL illumination for 10 days.

Time	Electrolyte	V_{oc} (mV)	J_{sc} (μA/cm^2)	*FF* (%)	Output Power (μW/cm^2)	η (%)
Day 1	dmby-4	594.9 ± 2.0	59.2 ± 0.1	45.6 ± 0.5	16.1	5.24 ± 0.1
	dmby-5	688.4 ± 1.6	85.9 ± 1.5	76.7 ± 0.7	45.4	14.8 ± 0.1
Day 2	dmby-4	661.8 ± 4.6	66.1 ± 1.1	44.3 ± 0.4	19.4	6.3 ± 0 .2
	dmby-5	726.7 ± 2.5	85.3 ± 1.5	75.8 ± 1	47	15.3 ± 0.1
Day 3	dmby-4	654 ± 1.4	67.2 ± 2.7	39.3 ± 0.7	17.3	5.6 ± 0.3
	dmby-5	728.9 ± 1	76.9 ± 1.3	74.4 ± 1.4	41.7	13.6 ± 0.5
Day 4	dmby-4	657.0 ± 1.1	62.2 ± 0.9	39.6 ± 0.8	16.2	5.3 ± 0.1
	dmby-5	726.1 ± 1.3	72.2 ± 1.8	72.9 ± 1.3	38.2	12.5 ± 0.1
Day 5	dmby-4	661.7 ± 13.8	66.3 ± 1	40.1 ± 3.9	17.6	5.7 ± 0.7
	dmby-5	727.6 ± 0.6	72.2 ± 0.7	72.4 ± 2.3	38.0	12.4 ± 0.4
Day 6	dmby-4	660.2 ± 0.9	63.8 ± 0.1	39.3 ± 0.3	16.6	5.4 ± 0.1
	dmby-5	730.1 ± 1.7	68.3 ± 1.3	71.7 ± 3.7	35.7	11.7 ± 0.8
Day 10	dmby-4	680.4 ± 0.8	64 ± 0.1	42 ± 0.3	18.3	6 ± 0.1
	dmby-5	741.7 ± 0.8	68.6 ± 0.1	71.3 ± 3.2	36.3	11.8 ± 0.5

Table S9 Comparison of photovoltaic result obtained from the present work with the best literature reports on indoor DSCs using organic dye-copper electrolyte combination under standard 1000 lux CFL illumination.

Sl.No	Light Intensity (lux)	J_{sc} (μA/cm^2)	V_{oc} (mV)	FF	η (%)	Dyes	Year	Reference
1	1000	134.9	905.3	0.8	35.6	D35:XY1	2023	**Present work**
2	1200	141.2	897.3	0.9	26.6	CXC22	2022	7
3	1000	144	660	0.7	21.6	Y123	2022	8
4	1000	138	980	0.8	34.5	MS5:XY1b	2021	9
5	1000	131.2	860	0.8	29.2	XY1:5T	2020	10
6	1000	147	910	0.77	34	XY1:L1	2020	11
7	1000	103	939	0.7	21.9	L156	2019	12
8	1000	149.3	878	0.8	31.8	Y123:XY1b	2018	13
9	1000	138	797	0.8	28.9	D35:XY1	2017	14

Table S10 Comparison of the best photovoltaic results obtained using D35:XY1 co-sensitized dyes and dual species dmp-5 electrolyte ($[Cu(dmp)_2]^+$/ $[Cu(dmp)_2Cl]^+$) from the present work with the best reported literature report using the similar co-sensitized dye under standard 1000 lux CFL illumination using $[Cu(tmby)_2]^{2+/+}$ electrolyte.

Sl.No	**Light Intensity**	**J_{sc} ($\mu A/cm^2$)**	**V_{oc} (mV)**	**FF (%)**	**η (%)**	**Electrolyte**	**Year**	**Reference**
1	1000	134.9	905.3	82.6	35.6	$[Cu(dmp)_2]^+$/ $[Cu(dmp)_2Cl]^+$	2023	**Present work**
2	1000	138	797	80.0	28.9	$[Cu(tmby_2]^{2+/+}$	2017	**14**

Table S11 Photovoltaic parameters of D35:XY1 co-sensitized DSCs using dmp-4, dmp-5, dmby-4 and dmby-5 electrolytes measured under different warm white CFL illumination intensities (500 lux, 200 lux and 50 lux).

Input Power ($\mu W/cm^2$)	Electrolyte	V_{oc} (mV)	J_{sc} ($\mu A/cm^2$)	*FF* (%)	Output Power ($\mu W/cm^2$)	η (%)
500 lux (143.05)	dmp-4	853.7 ± 5.6	41 ± 0.1	67.6 ± 0.2	23.7	16.5 ± 0.1
	dmp-5	878.4 ± 4	61.3 ± 0.1	81.2 ± 1.1	43.8	30.6 ± 0.3
	dmby-4	714.9 ± 1.1	35.3 ± 0.1	58.2 ± 0.3	14.7	10.3 ± 0.1
	dmby-5	760 ± 1.5	46 ± 0.1	69.9 ± 0.1	24.5	17.1 ± 0.1
200 lux (59.11)	dmp-4	704.7 ± 0.2	14.7 ± 0.1	66.2 ± 0.3	6.9	11.6 ± 0.1
	dmp-5	841.5 ± 0.9	24 ± 0.1	79.2 ± 0.2	16	27.1 ± 0.2
	dmby-4	630.1 ± 3.9	12.6 ± 0.1	37.6 ± 0.9	3	5 ± 0.2
	dmby-5	692.8 ± 0.2	17 ± 0.1	69.9 ± 0.2	8.2	13.9 ± 0.1
50 lux (12.03)	dmp-4	628.7 ± 1.1	4.3 ± 0.1	35.5 ± 0.7	1	8 ± 0.3
	dmp-5	748.5 ± 0.3	5.3 ± 0.1	69.5 ± 0.2	2.8	23 ± 0.1
	dmby-4	31 ± 0.1	3.7 ± 0.1	18.5 ± 0.1	0.1	0.2 ± 0.1
	dmby-5	598.5 ± 0.9	4.7 ± 0.1	61.2 ± 0.5	1.7	14.3 ± 0.2

Supplementary references

1 Y. Saygili, M. Söderberg, N. Pellet, F. Giordano, Y. Cao, A. B. Muñoz-García, S. M. Zakeeruddin, N. Vlachopoulos, M. Pavone, G. Boschloo, L. Kavan, J.-E. Moser, M. Grätzel, A. Hagfeldt and M. Freitag, *J. Am. Chem. Soc.*, 2016, **138**, 15087–15096.

2 Y. Wang and T. W. Hamann, *Chem. Commun.*, 2018, **54**, 12361–12364.

3 T. D. Kühne, M. Iannuzzi, M. Del Ben, V. V Rybkin, P. Seewald, F. Stein, T. Laino, R. Z. Khaliullin, O. Schütt, F. Schiffmann, D. Golze, J. Wilhelm, S. Chulkov, M. H. Bani-Hashemian, V. Weber, U. Borštnik, M. Taillefumier, A. S. Jakobovits, A. Lazzaro, H. Pabst, T. Müller, R. Schade, M. Guidon, S. Andermatt, N. Holmberg, G. K. Schenter, A. Hehn, A. Bussy, F. Belleflamme, G. Tabacchi, A. Glöß, M. Lass, I. Bethune, C. J. Mundy, C. Plessl, M. Watkins, J. VandeVondele, M. Krack and J. Hutter, *J. Chem. Phys.*, 2020, **152**, 194103.

4 K. Boguslawski, C. R. Jacob and M. Reiher, *J. Chem. Phys.*, 2013, **138**, 044111.

5 J. VandeVondele and J. Hutter, *J. Chem. Phys.*, 2007, **127**, 114105.

6 S. Grimme, J. Antony, S. Ehrlich and H. Krieg, *J. Chem. Phys.*, 2010, **132**, 154104.

7 C. Chen, V. S. Nguyen, H. Chiu, Y. Chen, T. Wei and C. Yeh, *Adv. Energy Mater.*, 2022, **12**, 2104051.

8 L. Li, L. Zhao, X. Jiang, Z. Yu, J. Liu, H. Rui, J. Shen, W. Sharmoukh, N. K. Allam and L. Sun, *J. Mater. Chem. A*, 2022, **10**, 4131–4136.

9 D. Zhang, M. Stojanovic, Y. Ren, Y. Cao, F. T. Eickemeyer, E. Socie, N. Vlachopoulos, J.-E. Moser, S. M. Zakeeruddin, A. Hagfeldt and M. Grätzel, *Nat. Commun.*, 2021, **12**, 1777.

10 E. Tanaka, H. Michaels, M. Freitag and N. Robertson, *J. Mater. Chem. A*, 2020, **8**, 1279–1287.

11 H. Michaels, M. Rinderle, R. Freitag, I. Benesperi, T. Edvinsson, R. Socher, A. Gagliardi and M. Freitag, *Chem. Sci.*, 2020, **11**, 2895–2906.

12 P. Ferdowsi, Y. Saygili, F. Jazaeri, T. Edvinsson, J. Mokhtari, S. M. Zakeeruddin, Y. Liu, M.

Grätzel and A. Hagfeldt, *ChemSusChem*, 2020, **13**, 212–220.

13 Y. Cao, Y. Liu, S. M. Zakeeruddin, A. Hagfeldt and M. Grätzel, *Joule*, 2018, **2**, 1108–1117.

14 M. Freitag, J. Teuscher, Y. Saygili, X. Zhang, F. Giordano, P. Liska, J. Hua, S. M. Zakeeruddin, J.-E. Moser, M. Grätzel and A. Hagfeldt, *Nat. Photonics*, 2017, **11**, 372–378.